AD-A061 415 NAVAL POSTGRADUATE SCHOOL MONTEREY CALIF F/G 8/10
THE FREQUENCY-DEPENDENT RESPONSE AND ASYMPTOTIC PROPERTIES OF T--ETC(U)
SEP 78 J YUN

UNCLASSIFIED NL

1 OF 1
AD
A061 415

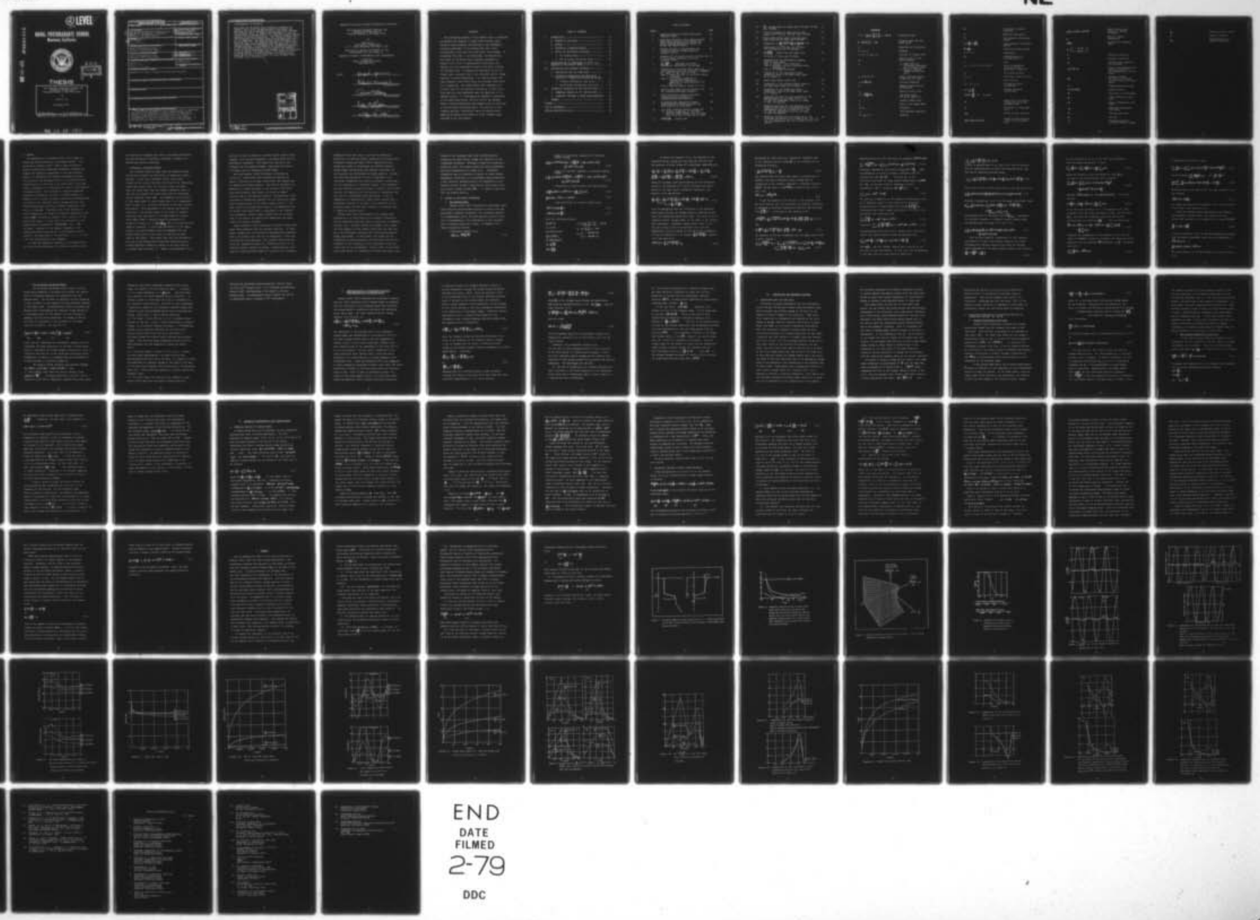

END
DATE
FILMED
2-79
DDC

(2) LEVEL II

NW

NAVAL POSTGRADUATE SCHOOL

Monterey, California

THESIS

THE FREQUENCY-DEPENDENT RESPONSE AND ASYMPTOTIC PROPERTIES OF TURBULENT MIXING IN THE UPPER OCEAN

by

Jae-Yul Yun

September 1978

Thesis Advisor: R. W. Garwood Jr.

Approved for public release; distribution unlimited

SECURITY CLASSIFICATION OF THIS PAGE (When Data Entered)

REPORT DOCUMENTATION PAGE

READ INSTRUCTIONS BEFORE COMPLETING FORM

1. REPORT NUMBER
2. GOVT ACCESSION NO.
3. RECIPIENT'S CATALOG NUMBER

4. TITLE (and Subtitle)
(6) The Frequency-Dependent Response and Asymptotic Properties of Turbulent Mixing in the Upper Ocean,

5. TYPE OF REPORT & PERIOD COVERED
(9) Master's Thesis; September 1978

6. PERFORMING ORG. REPORT NUMBER

7. AUTHOR(s)
(10) Jae-Yul Yun

8. CONTRACT OR GRANT NUMBER(s)

9. PERFORMING ORGANIZATION NAME AND ADDRESS
Naval Postgraduate School
Monterey, California 93940

10. PROGRAM ELEMENT, PROJECT, TASK AREA & WORK UNIT NUMBERS

11. CONTROLLING OFFICE NAME AND ADDRESS
Naval Postgraduate School
Monterey, California 93940

(11) 12. REPORT DATE
September 1978

13. NUMBER OF PAGES

14. MONITORING AGENCY NAME & ADDRESS(if different from Controlling Office)
(12) 88 p.

15. SECURITY CLASS. (of this report)
Unclassified

15a. DECLASSIFICATION/DOWNGRADING SCHEDULE

16. DISTRIBUTION STATEMENT (of this Report)
Approved for public release; distribution unlimited

17. DISTRIBUTION STATEMENT (of the abstract entered in Block 20, if different from Report)

18. SUPPLEMENTARY NOTES

19. KEY WORDS (Continue on reverse side if necessary and identify by block number)

20. ABSTRACT (Continue on reverse side if necessary and identify by block number)
The underlying purpose of this research was to understand and predict the response of upper ocean boundary layer mixing to high frequency oscillations in the atmospheric forcing attributable to the diurnal heat flux cycle, unsteadiness in the wind, and other short term changes. To accomplish this task, a non-stationary, one-dimensional

CONT

DD FORM 1 JAN 73 1473 EDITION OF 1 NOV 65 IS OBSOLETE
S/N 0102-014-6601

251 450

78 11 13 058

SECURITY CLASSIFICATION OF THIS PAGE (When Data Entered)

(continuation of abstract)

bulk model of the mixed layer originally proposed by Garwood (1976, 1977) is generalized by deriving a new equation for the entrainment buoyancy flux which includes the unsteady term. To examine the importance of the unsteady term, a reduced form of the turbulent kinetic energy equation is solved numerically. The results predict the high frequency cutoff above which the unsteady term should not be neglected. The quasi-steady state assumption is accurate only for low frequency forcing up to this cutoff. There was also some dependence upon the amplitude of the imposed forcing. To investigate the asymptotic properties of the mixed layer model, the full form of the Garwood model is solved numerically and compared with the solutions to the de Szoeke and Rhines model. The results of this research provide a theoretical basis for realistically applying the mixed layer models to ocean boundary layer problems on all time scales.

Approved for public release; distribution unlimited

The Frequency-Dependent Response and Asymptotic Properties of Turbulent Mixing in the Upper Ocean

by

Jae-Yul Yun
Lieutenant, Korean Navy
B. S., Seoul National University, 1974

Submitted in partial fulfillment of the
requirements for the degree of

MASTER OF SCIENCE IN METEOROLOGY AND OCEANOGRAPHY

from the
NAVAL POSTGRADUATE SCHOOL
September 1978

Author Jaeyul Yun

Roland W. Garwood Jr
Thesis Advisor

Russell L Elsberry
Second Reader

Dale F. Leipper
Chairman, Department of Oceanography

William M. Tolles
Dean of Science and Engineering

ABSTRACT

The underlying purpose of this research was to understand and predict the response of upper ocean boundary layer mixing to high frequency oscillations in the atmospheric forcing attributable to the diurnal heat flux cycle, unsteadiness in the wind, and other short term changes. To accomplish this task, a non-stationary, one-dimensional bulk model of the mixed layer originally proposed by Garwood (1976, 1977) is generalized by deriving a new equation for the entrainment buoyancy flux which includes the unsteady term. To examine the importance of the unsteady term, a reduced form of the turbulent kinetic energy equation is solved numerically. The results predict the high frequency cutoff above which the unsteady term should not be neglected. The quasi-steady state assumption is accurate only for low frequency forcing up to this cutoff. There was also some dependence upon the amplitude of the imposed forcing. To investigate the asymptotic properties of the mixed layer model, the full form of the Garwood model is solved numerically and compared with the solutions to the de Szoeke and Rhines model. The results of this research provide a theoretical basis for realistically applying the mixed layer models to ocean boundary layer problems on all time scales.

TABLE OF CONTENTS

I. INTRODUCTION ---------- 13

A. PURPOSE OF THE STUDY ---------- 13

B. METHOD ---------- 14

C. HISTORICAL LITERATURE REVIEW ---------- 15

D. REVIEW OF THE RECENT LITERATURE ---------- 18

1. The Garwood Model ---------- 18

2. The de Szoeke and Rhines Model -------- 28

II. GENERALIZATION OF ENTRAINMENT BUOYANCY FLUX EQUATION OF THE GARWOOD MODEL ---------- 31

III. DISSIPATION AND FREQUENCY RESPONSE ----------

A. DISSIPATION AND ITS TIME SCALE ---------- 35

B. SUBJECTIVE EXPECTATION AND ANALYTICAL SOLUTION TO INTERACTION BETWEEN τ_e AND τ_ε -- 37

1. Constant Dissipation Time Scale ------- 37

2. Non-Constant Dissipation Time Scale --- 39

IV. ASYMPTOTIC PROPERTIES OF THE GARWOOD MODEL ----- 44

A. NUMERICAL RESULTS OF THE GARWOOD MODEL ----- 44

B. ASYMPTOTIC REGIMES IN MIXED LAYER DEEPENING 48

V. SUMMARY ---------- 58

FIGURES ---------- 62

LIST OF REFERENCES ---------- 83

INITIAL DISTRIBUTION LIST ---------- 85

LIST OF FIGURES

Figure		Page
1	Idealized model for ocean mixed layer (Garwood (1976)).	62
2	Numerical solution of the complete mixed layer model equation of de Szoeke and Rhines showing asymptotic regimes (de Szoeke and Rhines (1976)).	63
3	General solution to entrainment and turbulent kinetic energy equations (Garwood (1977)).	64
4	Response of the mixed layer to fluctuations in the surface boundary conditions (Garwood (1976)).	65
5	$\frac{h}{u_*^3}\frac{d\langle \bar{E} \rangle}{dt}$ versus ωt for three frequencies $\omega h/u_* = 200\pi$, 2π and $.02\pi$	66
6	Comparison of following three cases for each nondimensionalized frequency (a) $\omega h/u_* = 200\pi$ (b) 2π and (c) $.02\pi$. Case 1) $\sin\omega t$ function of the wind forcing versus ωt. Case 2) fluctuating component of dissipation normalized in amplitude of wind production vs. ωt for a=1. Case 3) Same as case 2) except for a=.1.	67
7	Peak-to-peak amplitude of unsteady term vs. nondimensionalized frequency	68
8	Phase difference between wind shear production and dissipation vs. nondimensionalized frequency	68
9	Nondimensional dissipation versus prescribed wind shear production for four periods of oscillation	69
10	(a) Total turbulent kinetic energy and (b) vertical component of turbulent kinetic energy versus time for lapse rate $1^{\circ}C/2.5m$, $1^{\circ}C/25m$ and $1^{\circ}C/250m$.	70
11	$\langle \overline{w'^3} \rangle / \langle \bar{E} \rangle$ versus time	71

12	$\Delta\bar{b}$ versus time for lapse rate $1^{o}C/2.5m$, $1^{o}C/25m$ and $1^{o}C/250m$	72
13	$\bar{u}$ and $\bar{v}$ component of mean velocity for lapse rate $1^{o}C/2.5m$, $1^{o}C/25m$, and $1^{o}C/250m$	73
14	Mixed layer depth versus time for lapse rate $1^{o}C/2.5m$, $1^{o}C/25m$, and $1^{o}C/250m$.	74
15	Comparison of $\frac{dh}{dt}/\langle \overline{w^3} \rangle^{2/3}$, $\frac{dh}{dt}/u_*$, $\frac{dh}{dt}/\langle \bar{\varepsilon} \rangle$ for lapse rate (a) $1^{o}C/2.5m$, (b) $1^{o}C/25m$, (c) $1^{o}C/250m$ and (d) $1^{o}C/250000m$	75
16	$Ri^{-1} = \frac{\bar{u}^2 + \bar{v}^2}{h\Delta\bar{b}}$ versus time for lapse rate $1^{o}C/2.5m$, $1^{o}C/25$ m and $1^{o}C/250m$	76
17	Comparison of the entrainment damping term in three cases Case 1) Garwood - full equations Case 2) Garwood - without planetary scale dissipation Case 3) de Szoeke and Rhines	77
18	Comparison of the entrainment shear production term in the same three cases as in figure 17	77
19	Mixed layer depth versus time	78
20	Comparison of the nonstationarity term in the same three cases as in figure 17	79
21	Comparison of the production minus dissipation term in the same three cases as in figure 17	79
22	Numerical solution for the equations of the Garwood model (a) in terms of (A), (B), (C) and (D) separately, and (b) in terms of B/A, C/A and D/A	80
23	Numerical solution for the equations of the Garwood model without the planetary scale dissipation term (a) in terms of (A), (B), (C) and (D) separately, and (b) in terms of B/A, C/A and D/A	81
24	Numerical solution for the equations of the de Szoeke and Rhines (a) in terms of (A), (B), (C) and (D) separately, and (B) in terms of B/A, C/A and D/A.	82

NOTATION

$(\overline{\ }) = \lim_{L\to\infty} \frac{1}{L^2} \int_{-L/2}^{L/2} \int_{-L/2}^{L/2} (\ )\, dx\, dy$	Horizontal mean
$\langle (\ ) \rangle = \frac{1}{h} \int_{-h}^{0} (\ )\, dz$	Vertical mean over the mixed layer
a	Amplitude of fluctuation
$b = \bar{b} + b'$	Buoyancy
$c = \bar{c} + c'$, $c = u + iv$	Velocity in complex form
c_p	Specific heat at constant pressure
d	(1) Ekman depth of frictional resistance for the upper ocean (2) Depth of surface energy perturbation zone
$E = u'^2 + v'^2 + w'^2$	Total turbulent kinetic energy per unit mass
$f = 2 \lvert \vec{\Omega} \rvert \sin\phi$	Coriolis parameter
g	Apparent gravitational acceleration
h	Depth of mixed layer
$H^* = \frac{-\overline{b'w'}(0)h}{u_*^3}$	The mixed layer stability parameter
L	Obukhov length scale
l	Size of the large eddies
m, m_o	Constants
N	Brunt-Väisälä frequency
$P = pg + P'$	Pressure

P_g	Geostrophic pressure component
Q	Radiation absorption
Ri	Bulk gradient Richardson number
$Ri = \frac{\partial \bar{b}}{\partial z} \Big/ \frac{\partial^2 \bar{u}}{\partial z^2}$	Local gradient Richardson number
$R_*^* = \frac{u_*}{hf}$	Frictional Rossby number
$T = \bar{T} + T'$	Temperature
T_β	Nondimensionalized forcing period
t	time
$u_i = (\bar{u} + u', \bar{v} + v', \bar{w} + w')$	Total instantaneous velocity (without geostrophic component)
u_*	Frictional velocity
U_g, V_g	Geostrophic wind velocity
W	Wind velocity
$x_i = (x, y, z)$	Rectangular space coordinates
$\alpha = \frac{1}{\rho_0} \frac{\partial \rho}{\partial T}$	Thermal expansion coefficient
$\Gamma = N^2 = \frac{\partial \bar{b}}{\partial z}$ for $z < -h - \delta$	
γ	Lapse rate of potential temperature above the inversion base
δ	Thickness of entrainment zone
δc_0	Excess surface velocity
$\Delta \bar{b} = \bar{b}(-h) - \bar{b}(-h-\delta)$	Change in mean buoyancy across the entrainment zone

$\lvert\Delta\vec{C}\rvert = \left((\Delta\bar{u})^2 + (\Delta v)^2\right)^{1/2}$	Mean velocity drop across the density interface
ϵ	Rate of viscous dissipation
$(\overline{\theta w'})_i$	Buoyancy at inversion base
$\Lambda = \begin{cases} 1 \; ; & \partial h/\partial t \geq 0 \\ 0 \; ; & \partial h/\partial t < 0 \end{cases}$	
μ	Molecular viscosity
ν	Kinematic viscosity
ρ	Instantaneous density of the sea water
$\rho_o = \rho(T_o, S_o)$	Density for representative values of salinity S_o and temperature T_o in the ocean
σ_w	Average standard deviation of vertical velocity within the mixed layer
τ	Nondimensionalized time
$\lvert\tau(t)\rvert = \rho_o u_*^2$	Surface stress
τ_e	Time scale of entrainment
τ_ϵ	Total dissipation time scale
$\tau_{\epsilon 1}$	Viscous dissipation time scale
$\tau_{\epsilon 2}$	Planetary dissipation time scale
τ_f	Forcing time scale
ϕ	Latitude
Ψ	Nondimensionalized turbulent kinetic energy

Ω_j	Earth's rotation vector
ω	Angular frequency
ω_*	Nondimensionalized angular frequency

ACKNOWLEDGEMENTS

The author wishes to express appreciation to Dr. R. W. Garwood, Department of Oceanography, Naval Postgraduate School, for his time, interest, and guidance throughout this study, and to Dr. R. L. Elsberry, Department of Meteorology, Naval Postgraduate School, for many helpful discussions and review of this thesis.

Appreciation is also expressed to Dr. R. L. Haney who steered his interest to this study.

I. INTRODUCTION

A. PURPOSE OF THE STUDY

The objective of this research was to study the one-dimensional mixed layer model of Garwood (1976, 1977) in terms of a possible generalization of the extrainment buoyancy flux equation and to examine the responses of the mixed layer turbulent energy intensity to the different amplitude and frequencies for wind-shear turbulence production. Because of the frequency dependence, the steady state ($\frac{\partial \langle \bar{E} \rangle}{\partial t} = 0$, where $\langle \bar{E} \rangle$ is the turbulent kinetic energy averaged over the mixed layer depth) or quasi-steady state ($\frac{\partial \langle \bar{E} \rangle}{\partial t} \simeq 0$) assumption is good in some frequency ranges but it is not possible in other ranges. Using a constant dissipation time scale, Garwood (1976) suggested that if the quasi-steady state assumption is made to facilitate the solution without filtering the surface boundary conditions, an incorrect high frequency response will not only be present but may bias the mean mixing trend.

A further objective of this study is to critically examine the asymptotic time regimes of the Garwood model in comparison with those of the de Szoeke and Rhines (1976) model. These two tasks will provide a theoretical basis for realistically applying the mixed layer model to ocean boundary layer problems on all time scales.

B. METHOD

The equations of the Garwood (1976, 1977) model are listed and their derivation is discussed briefly. The de Szoeke and Rhines (1976) work is also reviewed in order to provide the background information necessary to compare the asymptotic properties of the two different models. To generalize the Garwood entrainment buoyancy flux equation, the unsteady term of the turbulent kinetic energy equation at the base of the mixed layer, which was usually considered to be negligible by earlier investigators, is parameterized. For the study of frequency-dependent response to atmospheric forcing, the method applied by Garwood (1976) in which he used a reduced and nondimensionalized form of the turbulent kinetic energy equation, and solved analytically by using a constant dissipation time scale, is reviewed. This same form of the equation is solved numerically by using a non-constant dissipation time scale, $h/\langle\varepsilon\rangle^{*}$, provided by Garwood (1976), where h is the mixed layer depth. In this case, the solutions for nondimensionalized frequencies $\omega h/u_{*} = 200\pi$, 2π, $.2\pi$, and $.02\pi$, where ω is the angular frequency of the normalized wind forcing and u_{*} is the maximum friction velocity, and amplitudes of fluctuations a = 0.1. 0.5 and 1 for the wind production are compared.

To study the asymptotic properties, the Garwood model is first solved numerically for different stabilities and

its results are compared with those of de Szoeke and Rhines by using equivalent calibration constants, boundary conditions and initial conditions.

C. HISTORICAL LITERATURE REVIEW

The vertical fluxes of heat, salt and momentum across the sea-air interface are the source of almost all oceanic motions. In the fully turbulent oceanic mixed layer bounded by the sea-air interface above and by the dynamically stable water mass below, the vertical fluxes are large. Below the mixed layer they are usually negligibly small so that one can decouple the mixed layer from the underlying stable, quiescent water mass. The immediate local reaction of this mixed layer to those fluxes result in a homogeneous water column, i.e., vertical uniformity in the mean velocity and density. This adjustment of the density and velocity structure of the surface layers of the ocean to variable fluxes has been the subject of a large number of studies since Ekman (1905)'s treatise where he originated the concept of a depth, $d = 7.5(\sec^{-1})\frac{W}{(\sin\phi)^{\frac{1}{2}}}$ (W is the wind velocity and ϕ is latitude), of frictional resistance for the upper section of a wind stressed ocean and suggested that any surface mixed layer by the action of wind has the same order of this depth. This depth comes from the mathematical solution to the steady state horizontal momentum equation in which Reynold's stress is related to the mean shear by a constant eddy viscosity, K . Rossby and Montgomery (1935)

pointed out that the depth of a surface drift current layer, $h \propto u_* / f$ (f is Coriolis parameter), and Ekman depth are not necessarily comparable. Both depths are derived by considering only the momentum budget, neglecting the effects of buoyancy and the mechanical energy budget.

Munk and Anderson (1948) developed a simultaneous solution of steady-state heat and momentum profiles by using a viscosity and an eddy conductivity that depend upon the gradient Richardson number. They did not recognize the presence of a sharp interface at the bottom of the mixed layer and therefore their result is closer to Ekman's solution than to the physical reality. Kitaigorodsky (1960) concluded by dimensional analysis that the mixed layer depth must be proportional to the Obukhov length scale, L. The basic flaw in his steady state model is the assumption that the entire ocean mixed layer is analogous to the constant-flux atmospheric surface layer, because with his constant flux at the surface the mixed layer temperature and depth cannot both remain unchanged.

Kraus and Rooth (1961) developed a plausible steady state model based primarily upon the buoyancy equation. In their model, steady state is achieved by balancing solar radiation with a net surface heat loss due to evaporation, conduction and long wave back radiation. The unstable density profile above the compensation depth is a convective source of the turbulent kinetic energy for mixing. Recognizing the limitation in Kraus and Rooth model--no provision for a possible

downward surface heat flux, no account of mechanical production of turbulent kinetic energy and the steady state constraint--Kraus and Turner (1967) improved the one-dimensional model by considering the turbulent kinetic energy budget utilizing the two separate equations, the heat equation and the mechanical energy equation. Because the frictional generation of heat is negligible, the vertically integrated heat equation provides a relationship for the conservation of potential energy. They parameterized the mechanical production rate in terms of the friction velocity but neglected the viscous rate of dissipation and the effect of entrainment shear production. From the examination of observations, Turner (1969) deduced that a substantial fraction of the part of the work done by the wind which goes into the drift current is eventually used to deepen the surface layer.

Miropol'skiy (1970) and Denman (1973) assumed that dissipation is a fixed fraction of mechanical production and the remaining turbulent kinetic energy goes to downward buoyancy flux. Pollard, Rhines and Thompson (1973) apply the slab approach to the oceanic mixed layer but they complete the entrainment problem with a different mechanical energy requirement. In this model, the energy for the entrainment is derived directly from the mean flow and the intensity of the turbulence is not considered to have an active role in the entrainment. Niiler (1974) in his three layer model which is a combination of Kraus and Turner, and

Pollard et al considered that both turbulent kinetic energy and the mean kinetic energy are important in the entrainment mechanism. Although he added the entrainment production term, the surface production minus dissipation was still parameterized in terms of u_* . Therefore, dissipation was not permitted to adjust to other varying atmospheric conditions or to entrainment shear production. A more realistic parameterization for dissipation is not possible without actually computing the mixed layer turbulent kinetic energy intensity $\langle \bar{E} \rangle$. It cannot be done with only the surface scale u_*.

D. REVIEW OF THE RECENT LITERATURE

1. The Garwood Model

Garwood (1976, 1977) developed an ocean mixed layer model using the Navier-Stokes equation of motion with the geostrophic component eliminated, the continuity equation in incompressible water, the heat equation from the first law of thermodynamics, the conservation of salt equation, and a linearized equation of state. A summary of the modeled equations follows:

entrainment buoyancy flux,

$$-\overline{b'w'}(-h) = \frac{\langle w'^2 \rangle^{3/2} \langle \bar{E} \rangle}{h} \qquad (1\text{-}1)$$

budget for horizontal components of turbulent kinetic energy,

$$\frac{1}{2}\frac{d}{dt}(h\langle\overline{u'^2+v'^2}\rangle) = m u_*^3 - \frac{h\,\overline{b'w'}(-h)}{2R_i} - (\langle\bar{E}\rangle - 3\langle\overline{w'^2}\rangle)\langle\bar{E}\rangle^{1/2} - \frac{2}{3}(\langle\bar{E}\rangle^{1/2} + fh)\langle\bar{E}\rangle \tag{1-2}$$

budget for vertical component of turbulent kinetic energy,

$$\frac{1}{2}\frac{d}{dt}(h\langle\overline{w'^2}\rangle) = \frac{h\,\overline{b'w'}(-h)}{2} + \frac{h\,\overline{b'w'}(0)}{2} + (\langle\bar{E}\rangle - 3\langle\overline{w'^2}\rangle)\langle\bar{E}\rangle^{1/2} - \frac{1}{3}(\langle\bar{E}\rangle^{1/2} + fh)\langle\bar{E}\rangle \tag{1-3}$$

conservation of mean buoyancy and mean momentum

$$h\frac{d\langle\bar{b}\rangle}{dt} = -\overline{b'w'}(0) + \overline{b'w'}(-h) + \frac{\alpha g}{\rho_0 c_p}\int_{-h}^{0} Q\,dz \tag{1-4}$$

$$\frac{d}{dt}(h\langle\bar{c}\rangle) = -\overline{c'w'}(0) - f\langle c\rangle h \tag{1-5}$$

"jump conditions" at bottom of mixed layer

$$-\overline{b'w'}(-h) = \Delta\bar{b}\frac{dh}{dt}\Lambda \tag{1-6}$$

$$-\overline{c'w'}(-h) = \Delta\bar{c}\frac{dh}{dt}\Lambda \tag{1-7}$$

with the following notation:

$u_i = \bar{u}_i + u_i'$

$c = u + iv$

$E = u'^2 + v'^2 + w'^2$

$u_*^2 = |\overline{c'w'}(0)|$

$\bar{b} = (\rho_0 - \rho)g/\rho_0$

$\alpha = \frac{1}{\rho_0}\frac{\partial\rho}{\partial T}$

$R_i = \frac{h\Delta b}{|\Delta\vec{u}|^2}$

$(\bar{\ }) = \lim_{L\to\infty}\int_{-L/2}^{L/2}\int_{-L/2}^{L/2}(\ )\,dx\,dy$

$\langle(\ )\rangle = \frac{1}{h}\int_{-h}^{0}(\ )\,dz$

$\Lambda = \begin{cases} 1 & ; \partial h/\partial t \geq 0 \\ 0 & ; \partial h/\partial t < 0 \end{cases}$

To derive the equation (1-1), the equation of the turbulent kinetic energy per unit mass was derived from the equation of motion using the Boussinesque approximation,

$$\frac{\partial}{\partial t}\left(\frac{\bar{E}}{2}\right) + \frac{\partial}{\partial x_j}\left(\frac{\bar{E}}{2}\bar{u}_j\right) + \frac{\partial}{\partial x_j}\left(\overline{u_j'\frac{E}{2}}\right) + \overline{u_i'u_j'}\frac{\partial \bar{u}_i}{\partial x_j} = -\frac{\partial}{\partial x_i}\left(\overline{u_i'\frac{p'}{\rho_o}}\right)$$

$$+\overline{\frac{p'}{\rho_o}\frac{\partial u_i'}{\partial x_i}} + \nu\frac{\partial}{\partial x_i}\left(\overline{u_i'\frac{\partial u_i'}{\partial x_j}}\right) - \nu\overline{\frac{\partial u_i'}{\partial x_j}\frac{\partial u_i'}{\partial x_j}} + \overline{u_i'b'}\,\delta_{i3} \qquad (1\text{-}8)$$

Using the boundary layer approximation and the continuity equation, and assuming that viscous diffusion and dissipation of the mean kinetic energy are negligible, the equation (1-8) was written:

$$\frac{\partial}{\partial t}\left(\frac{\bar{E}}{2}\right) = -\frac{\partial}{\partial z}\left[\overline{w'\left(\frac{E}{2}+\frac{p'}{\rho_o}\right)}\right] - \left[\overline{u'w'}\frac{\partial \bar{u}}{\partial z} + \overline{v'w'}\frac{\partial \bar{v}}{\partial z}\right] + \overline{b'w'} - \epsilon \qquad (1\text{-}9)$$

where $\epsilon = -\nu\overline{\frac{\partial}{\partial x_j}\left(u_i'\frac{\partial u_i'}{\partial z}\right)}$.

With the assumption that the turbulence of the overlying mixed layer provides the energy needed to destabilize and erode the underlying stable water mass. The local (at z=-h) turbulent kinetic energy budget is the basis of the entrainment hypothesis. Assuming a quasi-steady state of z=-h, and that within an active entrainment zone, the most significant source of energy for mixing is the convergence of flux of turbulent kinetic energy $-\frac{\partial}{\partial z}\left[\overline{w'\left(\frac{E}{2}+\frac{p'}{\rho_o}\right)}\right]$, equation (1-9) was reduced to:

$$\overline{b'w'}(-h) = \frac{\partial}{\partial z}\left[\overline{w'\left(\frac{E}{2}+\frac{p'}{\rho_o}\right)}\right]_{-h} \qquad (1\text{-}10)$$

Estimating the time scale, τ_e, required to transport some of the turbulent kinetic energy, $\langle \bar{E} \rangle$, to the viscinity of the entraining interface,

$$-\frac{\partial}{\partial z}\left[\overline{w'\left(\frac{E}{2}+\frac{p'}{\rho_0}\right)}\right]_{-h} = \frac{\langle \bar{E} \rangle}{\tau_e} \qquad (1\text{-}11)$$

and assuming that the mixed layer depth is proportional to distance over which turbulent kinetic energy must be transported by the vertical component of turbulent velocity, $\langle \overline{w'^2} \rangle^{1/2}$, τ_e was taken to be $h/\langle \overline{w'^2} \rangle^{1/2}$ and therefore from (1-10) and (1-11).

$$\overline{b'w'}(-h) = \frac{\langle \overline{w'^2} \rangle \langle \bar{E} \rangle}{h} \qquad (1\text{-}1)$$

To get the equation (1-2) and (1-3), the equation (1-9) was first divided into the horizontal and vertical components by assuming an isotropic dissipative structure and recalling that $\overline{\frac{p'}{\rho_0}\frac{\partial u_i}{\partial x_i}} = 0$ is included in the equation (1-9),

$$\frac{1}{2}\frac{\partial \overline{(u'^2+v'^2)}}{\partial t} = -\frac{\partial}{\partial z}\left[\overline{w'\frac{(u'^2+v'^2)}{2}}\right] - \overline{u'w'}\frac{\partial \bar{u}}{\partial z} - \overline{v'w'}\frac{\partial \bar{v}}{\partial z} + \overline{\frac{p'}{\rho_0}\frac{\partial u'}{\partial x}} + \overline{\frac{p'}{\rho_0}\frac{\partial v'}{\partial y}} - \frac{2}{3}\epsilon \qquad (1\text{-}12)$$

and

$$\frac{1}{2}\frac{\partial \overline{w'^2}}{\partial t} = \frac{\partial}{\partial z}\left[\overline{w'\left(\frac{w'^2}{2}+\frac{p'}{\rho_0}\right)}\right] + \overline{\frac{p'}{\rho_0}\frac{\partial w'}{\partial z}} + \overline{b'w'} - \frac{1}{3}\epsilon \qquad (1\text{-}13)$$

the equation (1-12) was integrated over the range from $z = -h-\delta$ to $z = 0$ (Figure 1)

$$\frac{1}{2}\int_{-h-\delta}^{0}\frac{\partial \overline{(u'^2+v'^2)}}{\partial t}\,dz = -\int_{-h-\delta}^{0}\frac{\partial}{\partial z}\left[\overline{w'\left(\frac{u'^2+v'^2}{2}\right)}\right]dz - \int_{-h-\delta}^{0}\left[\overline{u'w'}\frac{\partial \bar{u}}{\partial z} + \overline{v'w'}\frac{\partial \bar{v}}{\partial z}\right]dz$$
$$+\int_{-h-\delta}^{0}\overline{\frac{p'}{\rho_0}\left(\frac{\partial u'}{\partial x}+\frac{\partial v'}{\partial y}\right)}\,dz - \frac{2}{3}\int_{-h-\delta}^{0}\epsilon\,dz \qquad (1\text{-}14)$$

Applying Leibnitz's rule and using the assumption $(\overline{u'^2+v'^2})(-h-\delta)=0$,

$$\int_{-h-\delta}^{0} \frac{\partial(\overline{u'^2+v'^2})}{\partial t}\,dz = \frac{d}{dt}\int_{-h-\delta}^{0}(\overline{u'^2+v'^2})\,dz = \frac{d}{dt}(h\langle\overline{u'^2+v'^2}\rangle) \qquad (1\text{-}15)$$

Defining a dissipation time scale as $\int_{-h-\delta}^{0}\epsilon\,dz = \frac{\langle\bar{E}\rangle}{\tau_\epsilon}$ under the assumption of locally isotropic turbulence and considering that $\tau_\epsilon^{-1} = \tau_{\epsilon 1}^{-1} + \tau_{\epsilon 2}^{-1}$ in which $\tau_{\epsilon 1}$ is the convective time scale of large eddies (proportional to $h/\langle\bar{E}\rangle^{1/2}$) and $\tau_{\epsilon 2}$ is the time scale of planetary rotation (proportion to f^{-1}), therefore $\tau_\epsilon^{-1} = \frac{\langle\bar{E}\rangle^{1/2}}{h} + f$ and

$$\int_{-h-\delta}^{0}\epsilon\,dz = \langle\bar{E}\rangle^{3/2} + fh\langle\bar{E}\rangle \qquad (1\text{-}16)$$

The vertical integration of the pressure redistribution term is an important source or sink term for the individual turbulent kinetic energy budget even though $\sum_{i=1}^{3}\frac{\overline{p'}\,\overline{\partial u_i'}}{\rho_0\,\partial x_i} = 0$. Following Rotta (1951), Lumley and Khajeh Nouri (1974), the equivalent bulk formulation was

$$\int_{-h-\delta}^{0}\frac{\overline{p'}\,\overline{\partial u_i'}}{\rho_0\,\partial x_i}\,dz = \langle\bar{E}\rangle^{1/2}(\langle\bar{E}\rangle - 3\langle\overline{u_i'^2}\rangle) \qquad (1\text{-}17)$$

Therefore, $$\int_{-h-\delta}^{0}\frac{\overline{p'\left(\frac{\partial u'}{\partial x}+\frac{\partial v'}{\partial y}\right)}}{\rho_0}\,dz = -\langle\bar{E}\rangle^{1/2}(\langle\bar{E}\rangle - 3\langle\overline{w'^2}\rangle) \qquad (1\text{-}18)$$

Following Kraus and Turner (1967), Denman (1973) and Niiler (1975), the shear production term was parameterized:

$$-\int_{-h-\delta}^{0}\left(\overline{u'w'}\frac{\partial\bar{u}}{\partial z} + \overline{v'w'}\frac{\partial\bar{v}}{\partial z}\right)dz = u_*^2|\delta\bar{C}_0| + \frac{|\Delta\bar{C}|}{2}\frac{dh}{dt} \qquad (1\text{-}19)$$

where $|\delta\bar{C}_0|$ was the "excess" surface mean velocity in the direction of the wind stress. In this case, the inhomogeneity of the mean velocity field cannot be neglected.

$$-\int_{-h-\delta}^{0}\left[\frac{\partial}{\partial z}\overline{w'\left(\frac{p'}{\rho_0}+\frac{E}{2}\right)}\right]dz = m' u_*^3$$

If $|\delta \bar{c}_0|$ is proportional to u_*, then (1-18) may be combined with the parameterized net input from breaking waves, less the loss to radiating internal waves;

$$-\int_{-h-\delta}^{0}\left[\frac{\partial}{\partial z}\left[\overline{w'\left(\frac{p'}{\rho_0}+\frac{E}{2}\right)}\right]+\overline{u'w'}\frac{\partial \bar{u}}{\partial z}+\overline{v'w'}\frac{\partial \bar{v}}{\partial z}\right]dz = m u_*^3+\frac{|\Delta \bar{c}|^2}{2}\frac{dh}{dt} \quad (1\text{-}20)$$

From (1-15), (1-16), (1-18) and (1-20), (1-14) was written as:

$$\frac{1}{2}\frac{d}{dt}\left(h\langle\overline{u'^2+v'^2}\rangle\right) = m u_*^3+\frac{|\Delta \bar{c}|}{2}\frac{dh}{dt}-\langle\bar{E}\rangle^{3/2}\left(\langle\bar{E}\rangle-3\langle w'^2\rangle\right)-\frac{2}{3}\left(\langle\bar{E}\rangle^{3/2}+fh\right)\langle\bar{E}\rangle \quad (1\text{-}2)$$

Similarly integrating (1-13) over the range from $z=-h-\delta$ to $z=0$.

$$\frac{1}{2}\int_{-h-\delta}^{0}\frac{d}{dt}\left(h\langle\overline{w'^2}\rangle\right)dz = \int_{-h-\delta}^{0}\left(\overline{b'w'}+\frac{\overline{p'}}{\rho_0}\frac{\partial \overline{w'}}{\partial z}\right)dz-\left.\overline{w'\left(\frac{w'^2}{2}+\frac{p'}{\rho_0}\right)}\right|_0$$

$$+\left.\overline{w'\frac{p'}{\rho_0}}\right|_{-h-\delta}-\frac{1}{3}\int_{-h-\delta}^{0}\epsilon\,dz$$

and assuming $w'=0$ at the surface and $\left.\overline{w'\frac{p'}{\rho_0}}\right|_{-h-\delta}$ negligible, the vertical component of turbulent kinetic energy budget was parameterized by using (1-16) and (1-17);

$$\frac{1}{2}\frac{d}{dt}\left(h\langle\overline{w'^2}\rangle\right) = \frac{h}{2}\left[\overline{b'w'}(0)+\overline{b'w'}(-h)\right]+\langle\bar{E}\rangle^{3/2}\left(\langle\bar{E}\rangle-3\langle\overline{w'^2}\rangle\right) \quad (1\text{-}3)$$
$$-\frac{1}{3}\left(\langle\bar{E}\rangle^{3/2}+fh\right)\langle\bar{E}\rangle$$

From the heat equation, conservation of salt equation and equation of state, the buoyancy equation was formed. Averaging this buoyancy equation and using the boundary layer approximation, the mean buoyancy equation was obtained:

$$\frac{\partial \bar{b}}{\partial t} = -\frac{\partial \overline{b'w'}}{\partial z}+\frac{\alpha g}{\rho_0 c_p}Q \quad (1\text{-}21)$$

To get the equation (1-4), (1-21) was first integrated over the range from $z=-h-\delta$ to $z=0$.

$$\int_{-h-\delta}^{0} \frac{\partial \bar{e}}{\partial t} dz = -\int_{-h-\delta}^{0} \frac{\partial \overline{\rho' w'}}{\partial z} dz + \frac{\alpha_s}{c_p} \int_{-h-\delta}^{0} Q \, dz \qquad (1\text{-}22)$$

Using the Leibnitz's rule and taking the limit $\frac{\delta}{h} \to 0$, the term on the left hand side can be written;

$$\int_{-h-\delta}^{0} \frac{\partial \bar{e}}{\partial t} dz = \frac{d}{dt} \int_{-h-\delta}^{0} \bar{\rho} \, dz - [-\bar{\rho}(-h-\delta)] \frac{d(-h-\delta)}{dt}$$
$$= \frac{d}{dt}(h\langle\bar{\rho}\rangle) - \bar{\rho}(-h-\delta) \frac{dh}{dt} \qquad (1\text{-}23)$$

Assuming $\overline{\rho' w'}(-h-\delta)=0$ and using $\Delta\bar{\rho} = \langle\bar{\rho}\rangle - \bar{\rho}(-h-\delta)$, (1-21) was written;

$$h \frac{d\langle\bar{q}\rangle}{dt} = -\Delta\bar{\rho} \frac{dh}{dt} - \overline{\rho' w'}(0) + \frac{\alpha_s}{c_p} \int_{-h}^{0} Q \, dz \qquad (1\text{-}24)$$

To get the jump condition (1-6), the equation (1-21) was integrated over the range from $z=-h$ to $z=0$ and from z to $z=0$, and these two integrated equations were solved simultaneously to eliminate $\frac{d\langle\bar{\rho}\rangle}{dt}$. Then the result was

$$\overline{\rho' w'}(z) = \overline{\rho' w'}(0)\left(1+\frac{z}{h}\right) - \left(\overline{\rho' w'}(-h) + \frac{\alpha_s}{c_p}\int_{-h}^{0} Q \, dz\right)\frac{z}{h}$$
$$- \frac{\alpha_s}{c_p}\int_{z}^{0} Q \, dz \qquad (1\text{-}25)$$

Similarly the integration of the equation (1-21) over the range from $z=-h-\delta$ to $z=-h$ with dropping the negligible solar radiation term and assuming $\overline{\rho' w'}(-h-\delta)=0$ and $\frac{\delta}{h}$ approaches zero led to

$$\int_{-h-\delta}^{-h} \frac{\partial \bar{e}}{\partial t} dz = -\overline{\rho' w'}(-h) \qquad (1\text{-}26)$$

By applying the Leibnitz's rule,

$$\int_{-h-\delta}^{-h} \frac{\partial \bar{c}}{\partial t} dz = \frac{d}{dt}\int_{-h-\delta}^{-h} \bar{c}\, dz - \left[\bar{c}(-h)\frac{d(-h)}{dt} - \bar{c}(-h-\delta)\frac{d(-h-\delta)}{dt}\right] \quad (1\text{-}27)$$

and by assuming $\lim_{\delta \to 0} \frac{d(\delta \langle \bar{c} \rangle)}{dt} \simeq 0$ and $\lim_{\delta \to 0} \frac{d\delta}{dt} = 0$,

$$\lim_{\delta \to 0} \int_{-h-\delta}^{-h} \frac{\partial \bar{c}}{\partial t} dz = \left[\bar{c}(-h) - \bar{c}(-h-\delta)\right]\frac{dh}{dt} = \Delta \bar{c} \frac{dh}{dt} \quad (1\text{-}28)$$

Therefore from (1-26) and (1-28), the jump condition (1-6) was obtained

$$-\overline{c'w'}(-h) = \Delta \bar{c} \frac{dh}{dt} \quad (1\text{-}6)$$

and using this relation the equation (1-24) can be written in the form of the equation (1-4).

Using the boundary layer approximation and dropping the negligible viscous terms, the equations of mean motion were combined into a complex form by using $\bar{\zeta} = \bar{u} + i\bar{v}$

$$\frac{\partial \bar{\zeta}}{\partial t} = -if\bar{\zeta} - \frac{\partial \overline{\zeta' w'}}{\partial z} \quad (1\text{-}29)$$

To get the equation (1-5), (1-29) was integrated vertically over the range from $z=-h-\delta$ to $z=0$ with the assumption of $\overline{c'w'}(-h-\delta) = 0$;

$$\frac{d}{dt}(h\langle \bar{c} \rangle) = -if h\langle \bar{\zeta} \rangle - \overline{c'w'}(0) \quad (1\text{-}5)$$

The jump condition (1-7) was obtained in a similar way as (1-6).

The most important aspect of this model was the ability to predict the year-around evolution of the mixed layer depth together with bulk properties. This model provides not only structural prediction but also predicts a changing layer depth because the entrainment model provides boundary conditions at the moving density interface. In addition to the non-linear dependency upon stability, he found a Rossby number - $R_o^* = u_*/(fh)$ - dependence for the entrainment rate in his nondimensional solution. This makes possible a cyclical steady state for the boundary layer without requiring unrealistic values of upwelling or lateral advection in a long term integration.

On short time scales of the order of a few days, the upper ocean, even at higher latitudes, exhibits significant baroclinc activity. The importance of shorter-period fluctuations in the surface buoyancy flux in modulating the long-term response has demonstrated the need to know the typical daily heating/cooling cycle, solar radiation, evaporation, conduction and back radiation as a function of season and geographical coordinates. Some of the most fruitful applications of this model lie in the link-up with other models, for example, joining with an ocean circulation model.

In summary Garwood suggested in his model that first, the planetary rotation is assumed to influence the dissipation for deeper mixed layers and enables a cyclical steady state on an annual basis. Secondly, the rate of

entrainment for the stable regime is not accurately reflected by a linear extrapolation of the unstable situations. This is particularly important in modeling the ocean boundary layer. Unlike the atmospheric boundary case, most of the solar radiation does not penetrate the layer. Therefore, downward turbulent heat flux in the oceanic boundary layer is as important as the upward flux during the course of both diurnal and annual cycles. The non-linearity of interface entrainment tendency parameter, which is greatest for stable surface boundary conditions, results in a modulation of the long-term trend of mixed layer depth by the diurnal component of surface heat flux. Thirdly, in this model buoyant production is somewhat more efficient than shear production as a source of energy for vertical mixing because of its unique effect on the vertical component of the turbulent velocity.

2. The de Szoeke and Rhines Model

The de Szoeke and Rhines (1976) study of initial mixed layer deepening is reviewed here because the results will be critically analyzed in a comparison with the Garwood model. The solution to impulsive initial deepening is most relevant to this research on high frequency response of the upper ocean. Following Niiler (1975), de Szoeke and Rhines (1976) investigated the turbulent energy balance of a wind-mixed layer (in the absence of solar heating) by adding a new term which represents the energy to spin-up the level of turbulence in the increment of the mixed layer dh in time dt. The equation is

$$\left\{ \frac{1}{2}N^2h^4 - \frac{2u_*^4}{f^2}(1-\cos ft) + C_0 u_*^2 h^2 \right\} \frac{dh}{dt} = 2m_0 u_*^3 h^2 \qquad (1\text{-}30)$$

(A) (B) (C) (D)

where term (A) represents the entrainment damping, term (B) represents the shear production at the base of mixed layer, term (C) represents the energy needed to spin-up the level of turbulence and term (D) is the turbulence production minus dissipation, in which it is assumed that the dissipation is a fixed fraction of turbulent production.

The results (using constants and parameter $m_0 = C_0 = 1$, $u_* = 1$ cm/sec, $f = 10^{-4}$ sec^{-1}, $\Gamma = N^2 = 10^{-4}$ sec^{-2}) were

i) For slightly later than the initial instant, since $\cos ft \simeq 1 - \frac{(ft)^2}{2}$, the shear production, term (B), can be reduced to $u_*^4 t^2$ and is negligible compared with other terms.

Assuming a negligible entrainment damping at this early stage, the balance (C)$\sim$(D) holds for small t. Initially it is a linear deepening, i.e., $\frac{dh}{dt} \propto u_*$ and this lasts for a fraction of a Brunt-Väisälä period ($\sim$100 sec). It attains a depth of 2$\sim$7m while the level of turbulence in the incipient layer spins up. The term (C) here represents a significant demand on the available turbulent energy only during the first Brunt-Väisälä period after initiating the mixing. After that, it may be safely neglected.

ii) For large t (about 100 sec to 1 hr), a balance holds between (A) and (D). After it starts deepening by turbulent energy, the entrainment damping term grows. A $t^{1/3}$ deepening emerges as the turbulent work done by the wind at the surface erodes heavy fluid from below and mixes it uniformly through the surface layer, raising the potential energy. This one-third power deepening proceeds from the same mechanism that was suggested by Kraus and Turner (1967)

iii) For still larger t (about 1 hr to 12 hr), a balance (A)$\sim$(B) holds approximately. The mean flow has been accelerating until after 20 to 120 mins at a depth of 5$\sim$20m, the production of turbulent energy by the shear at the base of the mixed layer dominate other sources and a $t^{1/2}$ deepening takes over. This $h \propto t^{1/2}$ was proposed by Pollard, Rhines and Thompson (1972).

iv) For later times, the Coriolis force swings the mean motion vector away from the surface stress direction,

reducing the entrainment shear production (term B) below the rate $u_*^4 t^2$ assumed above. As t increases substantially beyond $t = \pi/f$ (corresponding to the lapse of one-half pendulum day). An approximate balance between (A) and (D) is established again, leading to $t^{1/3}$ development.

II. GENERALIZATIONS OF ENTRAINMENT BUOYANCY FLUX EQUATION OF THE GARWOOD MODEL

Garwood (1976, 1977) developed the entrainment equation from the total turbulent kinetic energy budget by assuming that the turbulence of the overlying mixed layer provides the energy needed to destabilize and erode the underlying stable water mass. The total turbulent kinetic energy equation (1-9) at $z=-h$ is:

$$\frac{1}{2}\frac{\partial \bar{e}}{\partial t}\Big|_{-h} = -\frac{\partial}{\partial z}\left[\overline{w'\left(\frac{e}{2}+\frac{p'}{\rho_o}\right)}\right]_{-h} - \left[\overline{u'w'}\frac{\partial \bar{u}}{\partial z} + \overline{v'w'}\frac{\partial \bar{v}}{\partial z}\right]_{-h} + \overline{b'w'}\Big|_{-h} - \epsilon\Big|_{-h} \qquad (2\text{-}1)$$

The importance of the unsteady term in the atmospheric energy budget was demonstrated by Zilitinkevich (1975) in the case of weak stratification, and also suggested by Garwood (1976) for the oceanic planetary boundary layer. A more detailed study of the importance of this term will be in the next chapter. For the order of magnitude of the shear production term, Garwood (1977) found that shear production is a fixed fraction of buoyant damping in the entrainment zone. Zeman and Tennekes (1977) also suggested in their atmospheric planetary boundary layer model that shear production is absent if the wind shear across the inversion base is zero. Even if there is substantial shear, the effect of this term appears likely to be relatively small (Mahrt and Lenschow, 1976), because mechanical production

of turbulence tends to be largely balanced locally by viscous dissipation through the energy cascade mechanism (Tennekes and Lumley, 1972). Since the position ($z=-h$) of the entrainment zone of the oceanic planetary boundary layer is defined by the location where the turbulent kinetic energy vanishes, local dissipation is also assumed to be a fixed fraction of the flux convergence term, should it be significant in the energy budget. Therefore, following Garwood (1977), a balance holds among the flux convergence term, buoyancy damping term and unsteady term. The equation (2-1) is reduced to:

$$\frac{1}{2}\frac{\partial \bar{E}}{\partial t}\Big|_{-h} = -\frac{\partial}{\partial z}\left[\overline{w'\left(\frac{E}{2}+\frac{p'}{\rho_o}\right)}\right]_{-h} + \overline{b'w'}\Big|_{-h} \qquad (2\text{-}2)$$

Since the boundary erodes and retreats depending on the level of the intensity of the turbulent kinetic energy, it may be assumed that the level of turbulent kinetic energy at the moving interface remains unchanged in the first approximation. Therefore,

$$\frac{d\bar{E}}{dt}\Big|_{-h} = \frac{\partial \bar{E}}{\partial t}\Big|_{-h} + \frac{\partial \bar{E}}{\partial z}\frac{\partial z}{\partial t}\Big|_{-h} \simeq 0$$

or (2-3)

$$\frac{\partial \bar{E}}{\partial t}\Big|_{-h} = -\frac{\partial \bar{E}}{\partial z}\frac{\partial z}{\partial t}\Big|_{-h}$$

Assuming that the turbulent kinetic energy decreases linearly with depth in the mixed layer and using the finite difference approximation, (2-3) can be written:

$$\left.\frac{\partial \bar{E}}{\partial t}\right|_{-h} = -\frac{\Delta \bar{E}}{\Delta z}\frac{\partial(-h)}{\partial t} = \frac{(\langle \bar{E} \rangle - 0)}{-\frac{h}{2}-(-h)}\frac{\partial h}{\partial t} = \frac{2\langle \bar{E} \rangle}{h}\frac{\partial h}{\partial t}\Lambda \qquad (2\text{-}4)$$

where $\langle \bar{E} \rangle$ is the average value through the mixed layer. Employing the parameterization (1-11), $\tau_e = \frac{h}{\langle w'^2 \rangle^{3/2}}$, and the jump condition (1-6),

$$\frac{1}{2}\frac{2\langle \bar{E} \rangle}{h}\frac{\partial h}{\partial t}\Lambda = -\frac{\langle \bar{E} \rangle}{h\Delta b}\overline{b'w'}(-h) = \frac{\langle \bar{E} \rangle \langle \overline{w'^3} \rangle}{h} + \overline{b'w'}(-h)$$

and this forms

$$\overline{b'w'}(-h) = \frac{\langle \bar{E} \rangle \langle \overline{w'^3} \rangle^{2/3}}{h + \langle \bar{E} \rangle / \Delta b} \qquad (2\text{-}5)$$

This more general equation of entrainment buoyancy flux replaces the equation (1-1) of the section I.D.1 for the final closure.

Therefore, the entrainment buoyancy flux, and the rate of layer deepening from (1-6) are functions of the bulk values, or overall layer averages, of both the total turbulent kinetic energy and the relative distribution of this energy between the horizontal and vertical components. The advantages are two-fold:

i) The rate of deepening is an integral property--not just a function of the local properties of the turbulence field, which may be vanishingly small at $z = -h$ inspite of a significant rate of deepening.

ii) The relative distribution of turbulent energy among the three geometric components is taken into account. Being able to include the root-mean-square vertical velocity, $\langle \overline{w'^2} \rangle^{1/2}$, is particularly important in realistically treating layer "retreat", $\frac{dh}{dt} < 0$.

In the case where $h\Delta b \gg \langle \bar{E} \rangle$, equation (2-5) returns to (1-1) of the original model. On the other hand, in the case $\langle \bar{E} \rangle \gg h\Delta b$ which is the case of weak stratification comparing to turbulent intensity (2-5) reduces to $\frac{\partial h}{\partial t} = \langle \overline{w'^2} \rangle^{1/2}$. That is, if the stratification is close to the neutral lapse rate, the entrainment proceeds at a rate proportional to the root mean square vertical velocity, $\langle \overline{w'^2} \rangle$. The comparable situation in the Zeman and Tennekes model is that $\overline{\theta' w'}$ tends to zero as the lapse rate, γ , tends to 0 (adiabatic conditions). Thus the energy budget in the absence of shear term and dissipation terms becomes a balance between the unsteady term and flux convergence term i.e., $\frac{\partial h}{\partial t} \propto \sigma_w$ where σ_w is the average standard deviation of vertical velocity within the mixed layer and will scale with $\langle \overline{w'^2} \rangle^{1/2}$.

III. DISSIPATION AND FREQUENCY RESPONSE

A. DISSIPATION AND ITS TIME SCALE

Turbulence is always dissipative and this dissipation occurs through viscous shear stress doing deformation work, which increases the internal energy of the fluid at the expense of kinetic energy of the turbulence. When these local losses due to dissipation are balanced by the local inputs of energy, then the turbulent structure in a given shear flow might be in a state of dynamical equilibrium. Since the turbulence consists of fairly large velocity fluctuations governed by nonlinear equations, one may expect a behavior like that exhibited by simple nonlinear systems with limit cycles. In a rapid energy transfer situations in which past events do not dominate the dynamics, one may expect that this limit cycle type of equilibrium is governed by the local length scales and time scales of the mean flow. In this turbulent motion the largest eddies may be as big as the width of the flow, which may then be an appropriate length scale in the analysis of the interaction of the turbulent and the mean flows. Large eddies lose a significant fraction of their kinetic energy within one "turnover time", but a negligible fraction is directly dissipated. This implies that the nonlinear mechanism that makes small eddies out of large ones is as dissipative as its characteristic time permits.

The nonlinear mechanism is ultimately dissipative because it creates smaller and smaller eddies until the eddy sizes become so small that viscous dissipation of their kinetic energy is dominant (eddy Reynolds number of order one).

Since small-scale motions tend to have small time scales, one may assume that these motions are statistically independent of the relatively slow, large scale turbulence for a sufficiently large Reynolds number for the mean flow. Therefore, the small-scale motion should depend only on the rate at which the large-scale motion supplies energy and on the kinematic viscosity. Thus it is assumed that this rate of energy supply should be equal to the rate of dissipation. If the dissipation rate, ϵ , can be related to the length and velocity scales of the large scale turbulence, one can assume that the rate at which large eddies supply energy to small eddies is proportional to the reciprocal of the time scale of the large eddies and therefore viscous dissipation of energy can be estimated from the large-scale dynamics which do not involve viscosity.

The amount of kinetic energy per unit mass in the large-scale turbulence is proportional to $\overline{u_i'^2}$ and the eddy time scale is assumed to be proportional to $l/(\overline{u_i'^2})^{1/2}$ where l represents the size of the largest eddies or width of the flow. From this general idea, Garwood (1976,1977) derived a total dissipation time scale, $\tau_\epsilon^{-1} = \frac{\langle\epsilon\rangle^{1/2}}{h} + f$ (for

derivation see section I.D.1 and for more detail see Garwood (1977)) by including the planetary scale of dissipation. This is the integral time scale of the turbulence. Depending upon the time scale (τ_F) of the surface forcing (variation in atmospheric conditions), an interaction between two time scales might be expected.

B. SUBJECTIVE EXPECTATION AND ANALYTICAL SOLUTION TO INTERACTION BETWEEN τ_ϵ AND τ_F

1. Constant Dissipation Time Scale

Garwood (1976) developed a solution for forcing period much longer than the integral time scale of the turbulence. This solution is governed by the dissipation time scale (τ_ϵ). For these time scales one can assume a quasi-steady state so that (1-2) and (1-3) become diagnostic equations for $\langle \overline{w'^2} \rangle$ and $\langle \overline{u'^2 + v'^2} \rangle$. In this way, the entrainment buoyancy flux (Fig. 3) can be computed directly as a function of the surface fluxes of momentum and buoyancy. However, fluctuations in surface boundary conditions u_*^2 and $\overline{b'w'}(o)$ of sufficiently short period require the consideration of the unsteady terms.

A very simple model which can be solved analytically provides an indication of the importance of this unsteadiness and how it might be treated. In the simple model, only two large terms, shear production and dissipation, are balanced by the time rate change of the turbulent kinetic energy,

$$\frac{\partial \langle \bar{E} \rangle}{\partial t} + \frac{\langle \bar{E} \rangle}{\tau_\epsilon} = \frac{u_*^3}{h}(1 + a \sin \omega t) \qquad (3\text{-}1)$$

where "a" is the amplitude of fluctuation and $\omega = 2\pi/\tau_F$ as its frequency. Assuming that the dissipation time scale is constant and defining a dimensionless time, $\tau = t/\tau_\epsilon$,

a dimensionless turbulent kinetic energy, $\psi = \frac{h\langle \bar{E} \rangle}{u_*^3 \tau_\epsilon}$,

and frequency, $\omega_* = \tau_\epsilon \omega = 2\pi \tau_\epsilon / \tau_F$,

(3-1) is written;

$$\frac{\partial \psi}{\partial t} + \psi = 1 + a \sin(\omega_* t) \qquad (3\text{-}2)$$

For cyclical steady state, the analytical solution to (3-2) is

$$\psi = 1 + \left(\frac{a}{\omega_*^2 + 1}\right)(\sin \omega_* \tau - \omega_* \cos \omega_* \tau) \qquad (3\text{-}3)$$

For the case a=o, ψ =1 which is the non-cyclical steady state solution. For finite amplitude, a, the full solution (3-3) is needed. In terms of frequency, for the low frequency fluctuations, $\omega_* < \sim .5$ (i.e., long period compared with τ_ϵ), the approximation of quasi-steady state is satisfied. Depending upon the Rossby Number ($R_O^* = u_*/(fh)$) and the mixed layer stability parameter ($H_* = \frac{\overline{b'w'}(o)h}{u_*^3}$), this low frequency fluctuation corresponds to a fluctuation period of several hours or longer. From

the complete solution (3-3), the important aspect is the relative magnitude of the response associated with the fluctuating component (fig. 4). For very high frequencies, $\omega_* \gg 1$, the amplitude of the response is negligible. In other words, the high frequencies are filtered out. This becomes a possible cause of error in using observed winds to drive a model having an integration time step smaller than or comparable with τ_ϵ . If the quasi-steady state assumption is made to facilitate obtaining a solution, but without filtering or smoothing the surface boundary conditions, an incorrect high-frequency response will not only be present but it may bias the mean trend.

2. Non-constant Dissipation Time Scale

In this case the same simplified equation (3-1) is considered, but the dissipation time scale τ_ϵ is no longer constrained to be constant. Using the convective dissipation time scale $\tau_\epsilon = \frac{h}{\langle \bar{E} \rangle^{1/2}}$ of Garwood (1976), (3-1) becomes;

$$\frac{\partial \langle \bar{E} \rangle}{\partial t} = -\frac{\langle \bar{E} \rangle^{3/2}}{h} + \frac{u_*^3}{h}(1 + a \sin \omega t) \qquad (3\text{-}4)$$

To examine the significance of the unsteady term, equation (3-4) is first nondimensionalized by defining

$$\psi = \frac{\langle \bar{E} \rangle}{u_*^2} ,$$

$$\tau = \frac{u_* t}{h} ,$$

and $$\omega_* = \frac{\omega h}{u_*}$$

then (3-4) is transformed to:

$$\frac{\partial \psi}{\partial \tau} = -\psi^{3/2} + 1 + a \sin(\omega_* \tau) \qquad (3\text{-}5)$$

The equation (3-5) is solved numerically for several combinations at amplitude (a=0.1, 0.5 and 1), and angular frequency of forcing ($\frac{\omega h}{u_*} = 200\pi$, 20π , 2π , 0.2π, and 0.02π). Initial adjustment was achieved at about $\frac{u_* t}{h} = 4$. There is also a tendency that the higher the forcing frequency, $\frac{\omega h}{u_*}$, the shorter the initial adjustment period that is needed. At the early stage of the wind forcing, the change of turbulent kinetic energy is mostly due to the wind forcing itself. As the energy supply from the wind continues, and after an initial adjustment is achieved, the balance among the three terms is changed and becomes a function of the amplitude and frequency of the forcing.

Different responses of the unsteady term to different frequencies of forcing are shown in figure 5 a-b for the case of small (a=0.1) and large (a=1) amplitude fluctuations. For both amplitudes, there is a tendency for the mean value of the unsteady term, $\frac{h}{u_*^3} \frac{\partial \langle \bar{E} \rangle}{\partial t}$, to vary with frequency even though it is very small. This is seen more clearly in the case of small amplitude fluctuation (a=.1) because of the magnified scale for the small amplitude case. The mean value is a little above zero for high frequency and it approaches zero as the frequency is getting lower. This effect is also shown in figure 6 which

are plots of the case 1); $\sin \omega t$ function of the wind forcing versus ωt , case 2); fluctuating component of dissipation normalized on the amplitude of the wind production ($(\frac{\varepsilon}{u_*^3}-1)/a$) versus ωt for a=1, and case 3); same as case 2) except a=.1. Comparing the fluctuating component of dissipation, case 2) and 3), with the constant wind forcing case 1), for each of three frequencies, one can see that the higher the frequency, the smaller the fraction of wind production that is dissipated in the mean. In other words, more energy is stored in the mean to deepen the mixed layer.

Figure 7 shows the peak-to-peak amplitude of the unsteady term $\frac{h}{u_*^3}\frac{\partial \langle \bar{\varepsilon} \rangle}{\partial t}$ versus frequency $\frac{\omega h}{u_*}$ for three amplitudes of fluctuation a=1,0.5 and 0.1. For each case, the peak-to-peak amplitude is almost a constant close to 2,1 and .2 respectively over the frequency range $\frac{\omega h}{u_*} = 2\pi$ to 200π and it is negligibly small for the frequency range below $.02\pi$. Some interesting transition cases occur over the frequency range $\frac{\omega h}{u_*} = .02\pi$ to 2π in which the adjustment time scale and forcing time scale are comparable, and therefore interact. For relatively low-frequency surface forcing, $\frac{\omega h}{u_*} \leq .02\pi$ (nondimensionalized period $T_R = \tau_\varepsilon / t_\varepsilon \geq 100$), regardless of magnitude of oscillation amplitude, the turbulent kinetic energy budget is in a quasi-steady state, i.e., dissipation is nearly proportional to the wind shear production as indicated by

the negligible peak-to-peak amplitude of unsteady term, $\frac{h}{\omega}\frac{\partial \langle \tilde{E} \rangle}{\partial t}$. Therefore, for this case, (3-4) reduces to

$$\langle \tilde{E} \rangle = u_*^2 \left(1 + a \sin \omega t\right)^{2/3} \qquad (3\text{-}6)$$

For relatively small amplitude oscillations ($a < 0.5$), regardless of frequency, it may be reasonable to assume a quasi-steady state for many cases in which a high degree of accuracy is not required. But for relatively large amplitude oscillations, the unsteady term is more clearly frequency-dependent. For $a < 0.5$ and in the transition frequency range below $\frac{\omega h}{u_*} = .2\pi$, it may not still be a bad approximation to assume a quasi-steady state and use (3-6) in an approximate sense. On the other hand, for $a \geq .5$ and frequency $\frac{\omega h}{u_*} = .2\pi$, this unsteady term is no longer negligible. Therefore it is strongly suggested that the full form of equation (3-4) be used to avoid an incorrect high frequency response.

Figure 8 shows the phase difference between the wind forcing and the dissipation as a function of the frequency of the forcing. For the frequency range there is almost no phase shift. As shown by the negligible amount of hysteresis in figure 9a, the dissipation is nearly proportional to the wind shear production after the initial adjustment period $0 < \frac{u_* \zeta}{h} < 4$. In the other extreme of high frequency forcing ($\frac{\omega h}{u_*} > 20\pi$), there is almost a 90° phase shift between wind production and dissipation. As

shown in figure 9d, the adjustment period is longer relative to the forcing time scale, but dissipation converges to a constant value that is independent of the frequency and magnitude of the forcing oscillations. For the frequency range, $.02\pi < \frac{\omega h}{u_*} < 20\pi$, in which the two time scales are comparable, the phase shift increases nearly from zero at $.02\pi$ to nearly 90° at 20π . Figure 9b and 9c show that since the adjustment time scale and the forcing time scale are comparable and interact, this causes the ellipsoid to achieve a maximum width in this domain, $1 < T_F < 10$. An important result is revealed by figure 9b which shows that the amplitude of the response cycle is nearly proportional to the amplitude of the forcing cycle, inspite of the hysteresis. Therefore, if phase information is not crucial, it is accurate for this case to assume a quasi-steady state.

IV. ASYMPTOTIC PROPERTIES OF THE GARWOOD MODEL

A. NUMERICAL RESULTS OF GARWOOD MODEL

If quasi-steady state is not assumed, the full prognostic equations may still be solved numerically. The full equations of Garwood model, (2-5), (1-2), (1-3), (1-4) and (1-5) with the jump conditions (1-6) and (1-7) are solved numerically for about a one-day period using hypothetical initial conditions, h=1m, $\langle \bar{E} \rangle = .03\ cm^2/sec^2$, $\langle \overline{w'^2} \rangle = .01\ cm^2/sec^2$, $\bar{u}=0$, $\bar{v}=0$ and three different cases of $\Delta\bar{b}$ ($\Delta b = 5\times10^{-4}$, 5×10^{-3} and $5\times10^{-2}\ cm/sec^2$). The size of $\Delta\bar{b}$ indicates the degree of stratification and is related to the lapse rate, Γ, as follows;

$$\Delta\bar{b} = \frac{\Gamma h}{2} - \frac{1}{h}\int_0^t \overline{bw'}(0)\,dt \qquad (4\text{-}1)$$

where $\Gamma = \frac{\partial \bar{b}}{\partial z} \simeq \alpha g \frac{\partial T}{\partial z} \simeq .25 \frac{\Delta T}{\Delta z}$ for the simple case of vertically homogeneous salinity. Assuming the surface buoyancy flux to be negligible, $\overline{bw'}(0)=0$, $\Delta\bar{b} = 5\times10^{-4}\ cm/sec^2$ corresponds to $\frac{\Delta T}{\Delta z} = 1^\circ C/250\ m$ (i.e. $\Gamma = 10^{-5}\ sec^{-2}$). $\Delta\bar{b} = 5\times10^{-3} cm/sec^2$ corresponding to $\frac{\Delta T}{\Delta z} = 1^\circ C/25\ m$ (i.e. $\Gamma = 10^{-4}\ sec^{-2}$). The constant employed here is $m=6$. To simplify the problem, the momentum flux $\overline{u'w'}(0) = 1\ cm^2/sec^2$, $\overline{v'w'}=0$, the constant frictional velocity $u_* = 1\ cm/sec$, $Q=0$, $\overline{bw'}=0$ and $f = 10^{-4}\ sec^{-1}$ are also assumed. Using these conditions, three different curves of each parameter are plotted for each lapse rate.

Figure 10 shows that the stronger the stratification, the larger the amount of turbulent kinetic energy in the mixed layer. It starts from $\langle \bar{E} \rangle = .03\ cm^2/sec^2$ and very rapidly increases during a short period immediately following an impulsively applied surface forces. $\langle \bar{E} \rangle$ shows a maximum at t=3~5 hrs., a minimum at t=17~18 hrs. and a second maximum at t=24~25 hrs. The figure also shows that the weaker the stratification, the earlier the maximum is reached. The vertical component of turbulent kinetic energy shows a similar pattern except for the case of weak stratification ($\frac{\Delta T}{\Delta z} = 1°C/250\,m$) in which it decreases monotonically (fig. 10b). Figure 11 shows $\langle \overline{w'^2} \rangle / \langle \bar{E} \rangle$ versus time for $\frac{\Delta T}{\Delta z} = 1°C/2.5\,m$, $1°C/25\,m$ and $1°C/250\,m$. Starting with $\langle \overline{w'^2} \rangle / \langle \bar{E} \rangle = 0.33$, it reaches 0.15, 0.14 and 0.13 respectively after a one-day period. These sudden reductions in $\langle \overline{w'^2} \rangle / \langle \bar{E} \rangle$ occur at a very early stage and then stay nearly constant. In other words, vertical components of turbulent kinetic energy relative to total kinetic energy adjust rapidly in the early stages, and, the stronger the stratification, the larger will be the vertical component relative to total kinetic energy.

Figure 12 shows changes in $\Delta\bar{b}$ with time. Each $\Delta\bar{b}$ increases monotonically, although more rapidly in the case of stronger lapse rate. Larger values of $\Delta\bar{b}$ contribute to more turbulent damping due to mixing at the interface.

Figure 13 shows the change in current with time, and indicates that the stronger the stability, the larger will be its magnitude. With the imposed east wind, the currents start flowing westward at the initial instant. The west component reaches a maximum value of 17 cm/sec, with the northward component current still growing. As the west component decreases to zero, the north component current reaches a maximum of 25 cm/sec. This slowly turning current direction is caused by Coriolis force which deflects the current direction to the right in the Northern Hemisphere. After one inertal period, both $\bar{u}$ and $\bar{v}$ decrease to zero. The maximum of $\bar{u}^2 + \bar{v}^2$ occurs at about t=4hrs and the minimum is at about t=17hrs. Also the figure 13 shows that the magnitude of each successive maximum value decreases with time.

Figure 14 shows the monotonically increasing mixed layer depth with time. All cases start from 1m and after 10^5sec the mixed layer depth is 45m for $\frac{\Delta T}{\Delta z}$ = 1^{oC}/250m, 23m for $\frac{\Delta T}{\Delta z}$ = 1^{oC}/25m and 11m for $\frac{\Delta T}{\Delta z}$ = 1^{oC}/2.5m. These indicate that the larger the stability, the lesser the deepening it is.

Figure 15 a-c show $\frac{dh}{dt}/\langle \overline{w'^2} \rangle^{1/2}$, $\frac{dh}{dt}/u_*$ (or $\frac{dh}{dt}$ because $u_* = 1$ cm/sec is assumed) and $\frac{dh}{dt}/\langle E \rangle^{1/2}$ for each lapse rate. The middle curve of each figure indicates that $\frac{dh}{dt}$ decreases more rapidly in large stability than in weak stability. For each case, $\frac{dh}{dt}/\langle \overline{w'^2} \rangle^{1/2}$, $\frac{dh}{dt}/u_*$ and $\frac{dh}{dt}/\langle E \rangle^{1/2}$

are not parallel prior to about one inertial period, i.e., $\frac{dh}{dt} \propto \langle \overline{w'^2} \rangle^{1/2}$ and $\frac{dh}{dt} \propto u_*$ would not produce the same deepening even though $\overline{b'w'}(0) = 0$ is assumed. The figures imply that in general the deepening is not proportional to $\langle \overline{w'^2} \rangle^{1/2}$, $\langle \bar{\varepsilon} \rangle^{1/2}$ or u_*, but rather depends upon the full form of entrainment equation $\frac{dh}{dt} = \frac{\langle \bar{\varepsilon} \rangle \langle \overline{w'^2} \rangle^{1/2}}{\langle \bar{\varepsilon} \rangle + h \Delta \bar{b}}$. An exception occurs if $h \Delta \bar{b} \simeq 0$ so that $\frac{dh}{dt} = \langle \overline{w'^2} \rangle^{1/2}$ during the early stages (Figure 15d).

Figure 16 shows the inverse of the bulk Richardson number changing with time. For $t < 20$ mins, R_i^{-1} is large in the case of weak initial stability because of the small $\Delta \bar{b}$. After 20 mins, the larger values of R_i^{-1} occurs for the cases with larger initial stability. This is due to the strong mean shear developed at this stage. At one inertial period, R_i^{-1} goes to zero because of the stagnation in current at this moment. Halpern (1974) suggested that if local Richardson number ($R_{il} = \frac{\partial \bar{b}}{\partial z} / \frac{\partial^2 \bar{u}_i}{\partial z^2}$) is less than one-fourth, instability may occur, and if $R_{il} = 1$, marginal stability exists. He also suggested in his experimental study of Northern Pacific Ocean that $R_{il} = \frac{1}{4}$ is a critical condition for the occurence of shear instability. Therefore, for the case of $\frac{\Delta T}{\Delta z} = 1°C/250\,m$, there is an instability at about t=100sec. If R_{il}^{-1} is considered to be an average of R_{il}^{-1} over the mixed layer depth and therefore $R_i^{-1} > R_{il}^{-1}$, there may also be an instability at t=4hrs for the case of $\frac{\Delta T}{\Delta z} = 1°C/2.5\,m$. This instability leads to a maximum turbulent kinetic energy at this time interval.

Therefore, how the turbulence develops with time, as indicated by equation (1-2) and (1-3), can be summarized. The total turbulent kinetic energy (fig. 10) $\langle \bar{E} \rangle$ jumps due to impulsively applying surface stress to an initially resting fluid, whereas the energy produced by any mechanism is dissipated at a rate proportional to $\langle \bar{E} \rangle^{3/2}$. Then, the shear production is increased to a maximum value even though the damping also increases. The maximum turbulent kinetic energy exists at about t=4hrs, and then decreases toward a minimum mainly due to decreasing shear production at about one inertial period.

The more detailed, term-by-term study is left for the next section.

B. ASYMPTOTIC REGIMES IN MIXED LAYER DEEPENING

Combining equations (1-2) and (1-3) of the Garwood model, the total turbulent kinetic energy budget equation is obtained.

$$\frac{d(h\langle \bar{E} \rangle)}{dt} = 2m u_*^3 + |\Delta \vec{v}|^2 \frac{dh}{dt} + h\overline{b'w'}(0) - h\Delta b \frac{dh}{dt} - 2(\langle \bar{E} \rangle^{3/2} + fh\langle \bar{E} \rangle)$$

Using $h\Delta b = \frac{1}{2}N^2h^2$, one can write the above equation in the following order;

$$\underset{(A)}{\frac{1}{2}N^2h^2\frac{dh}{dt}} \underset{(B)}{-|\Delta \vec{v}|^2\frac{dh}{dt}} + \underset{(C)}{\frac{d(h\langle \bar{E} \rangle)}{dt}} = \underset{(D)}{2m u_*^3 - 2(\langle \bar{E} \rangle^{3/2} + fh\langle \bar{E} \rangle)} \quad (4\text{-}2)$$

The corresponding equation from de Szoeke and Rhines (1976) may be obtained by dividing equation (1-30) by h^2.

$$\left[\frac{1}{2}N^2h^2 - \frac{2u_*^4}{f^2h^2}(1-\cos ft) + c_0u_*^2\right]\frac{dh}{dt} = 2m_0u_*^3 \qquad (4\text{-}3)$$

(A) (B) (C) (D)

Equation (4-3) is originally the Niiler model except for the term (C). The term(A) in both (4-2) and (4-3) is an entrainment damping term which is a upward buoyancy flux at the base of this mixed layer. The term (B) in both equations is the shear production term. The term (C) in (4-3) is the energy needed to spin up the level of turbulence, $c_0u_*^2$, in the increment of mixed layer dh in time dt, while the term (C) in (4-2) is the nonstationarity term which shows the incremental change of the turbulent energy budget $d(h\langle\bar{\epsilon}\rangle)$ in time dt. The term (D) in both equations is the wind shear production minus dissipation. Before analyzing the numerical solutions it might be useful to examine the characteristics of both equations and their differences.

i) Both models contain nonlinear equations, i.e., the Garwood model is a set of six nonlinear differential equations which can be solved implicitly for each parameter, while the de Szoeke and Rhines model has one nonlinear differential equation.

ii) Both models have numerical problems when the zero-initial condition (h(t=0)=0) are used, although such conditions are not likely to occur in nature.

iii) The nonstationarity term in Garwood, $\frac{d(h\bar{E})}{dt} = h\frac{d\langle\bar{E}\rangle}{dt} + \langle\bar{E}\rangle\frac{dh}{dt}$ is not exactly comparable to $c_o u_*^2 \frac{dh}{dt}$ of de Szoeke and Rhines. Even with the assumption of no surface buoyancy flux, $\langle\bar{E}\rangle/u_*^2$ does not approach a constant for $\frac{\Delta T}{\Delta z} = 1°C/2.5m$, $\frac{\Delta T}{\Delta z} = 1°C/25m$ and $\frac{\Delta T}{\Delta z} = 1°C/250m$ up to one inertial period. After this period, $\langle\bar{E}\rangle/u_*^2$ = constant holds approximately, although it is still not exact except for the case of weak stratification (figure 10a). Even when the condition $\langle\bar{E}\rangle/u_*^2$ = constant holds, there is a difference of $h\frac{d\langle\bar{E}\rangle}{dt}$ between the two models.

iv) Term (D) in the Niiler (1975) model is parameterized in the manner;

$$-w'\left(\frac{p'}{\rho_o} + \frac{E}{2}\right)\Big|_o - \int_d^0 \overline{u'w'}\frac{\partial \bar{u}_1}{\partial z}\,dz - \int_d^0 \epsilon\,dz = m_o u_*^3$$

where "d" is the depth of the perturbation energy production zone near the surface. This implies that only the near surface production is dissipated. In other words, dissipation is a fraction of production term near the surface. None of the shear production energy at the base of mixed layer and the surface buoyancy production energy (this term is not considered for this study) goes to dissipation. Because of this parameterization, the shear production at the base of mixed layer has only an interaction with the entrainment damping term. On the other hand, in the Garwood model, dissipation is parameterized in a way that all the production including the entrainment shear production and the surface buoyancy flux is dissipated.

Term (D) in the Garwood model is the turbulent production over the whole depth minus the total dissipation, i.e., the viscous dissipation as well as the planetary scale dissipation. This second dissipation term is not included in the Niiler model. If the planetary scale dissipation is neglected and $\frac{\langle \bar{E} \rangle}{u_*^3}$ = a constant is considered, then term (D) in the Garwood model approaches term (D) in the de Szoeke and Rhines equation of the Niiler model within a constant factor.

With these characteristics and differences in mind, two cases of the Garwood model and one case of the de Szoeke and Rhines model are solved numerically using the same conditions.

Case 1) The equations (2-5), (1-2), (1-3), (1-4)and (1-5) with the jump conditions are solved numerically using the same constants and initial conditions as in the case of $\frac{\Delta I}{\Delta z} = 1°C/25m$ ($\Gamma = 10^{-4}\ sec^{-2}$) in Section IV.1 (i.e., Parameters and boundary conditions: $m=6$, $u_* = 1\ cm/sec$, $f = 10^{-4}\ sec^{-1}$ $\overline{u'w'}(0) = 1\ cm^2/sec^2$, $\overline{v'w'}(0)=0$, $\overline{b'w'}(0)=0$ and initial conditions: $h = 100\ cm$, $\langle \bar{E} \rangle = .03\ cm^2/sec^3$, $\langle \overline{w'^2} \rangle = .01\ cm^2/sec^2$, $\Delta \bar{b} = 5 \times 10^{-3}\ cm/sec^2$)

Case 2) is similar to case 1) except that there is no planetary scale dissipation term in (1-2) or (1-3).

Case 3) Equation (4-3) of de Szoeke and Rhines is solved numerically using $C_0 = m_0 = 1$, $u_* = 1\ cm/sec$, $f = 10^{-4}\ sec^{-1}$ and $\Gamma = N^2 = 10^{-4}\ sec^{-2}$.

Each solution is displayed from t=50sec because the initial values of terms (C) and (D) are large. The three cases of term (A) are plotted in Figure 17. Maximum

entrainment damping occurs at t=4~5 hrs and a second maximum at t=25 hrs for each case. The entrainment damping of the de Szoeke and Rhines model is twice as large as that of the Garwood model at the time of the first maximum and remains larger than that of the Garwood model throughout. Case 2) of the Garwood model and Case 3) of de Szoeke and Rhines are very close at time equal to one inertial period. The entrainment damping of Case 2) (i.e., without planetary scale dissipation) is larger than that of Case 1) of Garwood model after t=15 mins and the difference increases with time. For the time interval less than 15 mins, the planetary scale dissipation term does not make any contribution to the entrainment damping. The large damping of term (A) in the de Szoeke and Rhines equation compared to the Garwood model occurs inspite of the large shear production in the Garwood Model (Figure 18). This may be due to the fact that none of the shear production of the de Szoeke and Rhines equation dissipates. Instead, all of this energy goes to deepen the mixed layer, and therefore the entrainment damping grows larger to offset the larger entraining energy. The reason for larger damping in case 2) than in case 1) is because there is less dissipation in case 2) (without planetary scale dissipation) and thus there is more entraining energy available, against which entrainment damping grows. Since this planetary scale dissipation increases with time, the difference in the entrainment damping between the two cases also increases

with time. Since the entraining due to entrainment shear production decreases to zero (Figure 18) at one inertial period in all cases, the net entraining energy in case 2) and case 3) is the same at this time stage and therefore the entrainment damping in case 2) and case 3) is almost the same. Whereas, case 1) has less entraining energy because of planetary scale dissipation. This leads to less entrainment damping at this same time stage.

Figure 18 shows term (B) for the three cases. The figure shows that the entrainment shear production of the Garwood model is not affected by the planetary scale dissipation term and the term (B) of the Garwood model is larger than that of the de Szoeke and Rhines model at least for one-day period. It also shows that the time of maximum shear production agrees with the time of maximum entrainment damping as discussed in term (A). The reason for the smaller entrainment shear production of the de Szoeke and Rhines model is because there is no dissipation attributable to the entrainment shear production, and this leads to larger deepening in the de Szoeke and Rhines model than in the Garwood model (Figure 19). Therefore, the term (B) of the de Szoeke and Rhines model, which is divided by h^2, shows a smaller value of extrainment shear production.

Figure 20 shows the value of the (C) terms. Again, the planetary scale dissipation term of the Garwood model does not affect this term. This term in the Garwood model is

larger than that of the de Szoeke and Rhines, although the difference between the two models diminishes in time. The reason for term (C) (Figure 20) being larger in the case of the Garwood model, and possible for the decrease in the difference with time is because of the omission of the term, $h\frac{d\langle\bar{E}\rangle}{dt}$, in the de Szoeke and Rhines model. In addition, this is also because $\langle\bar{E}\rangle/u_*^2$ tends to be large at first and only becomes nearly constant after about an inertial period.

The last and important (D) terms are plotted in figure 21. The term (D) of de Szoeke and Rhines is equal to 2.0 and thus appears as a straight line. On the other hand, the term (D) for case 1) and case 2) of the Garwood model varies with time. After several minutes, the planetary scale dissipation term starts to act and because of this action, the term (D) of case 1) is always less than that of case 2) with larger differences at the maximum and minimum values. After one inertial period,case 2) and case 3) are close together, because there is no entrainment shear, therefore no dissipation of entrainment shear production (this is always the case for de Szoeke and Rhines) and no dissipation from planetary rotation in both cases. The larger differences of the term (D) between case 1) and case 2) at the time of minimum is because of the larger value of $\langle\bar{E}\rangle$ due to large entrainment shear production which contributes to larger planetary scale dissipation, .
The term (D) of the Garwood model shows a negative value

between t=1.3 hrs and t=10.1 hrs. The reason for this negative value during this time interval is because the term (D) is not a net production term, i.e., this term does not include the shear production at the base of the mixed layer but does include the dissipation from that entrainment shear production. Therefore, this term shows a minimum during this time interval whereas term (B) (Figure 18) shows its maximum.

To examine the asymptotic regimes, the solutions for case 1), case 2) and case 3) are plotted for separate (A), (B), (C), and (D) terms and also for B/A, C/A and D/A following de Szoeke and Rhines (see also Figure 2). However, since the results for case 1) and case 2) are almost the same, only case 1) will be considered. From the initial instant to about t=5 mins a balance (C)~(D) holds for the Garwood model (Figure 22).

$$\frac{d(h\langle\bar{E}\rangle)}{dt} \sim 2m u_*^3 - 2(\langle\bar{E}\rangle^{3/2} + f h\langle\bar{E}\rangle) \qquad (4\text{-}4)$$

This is similar to the balance in the de Szoeke and Rhines model except that the duration for their model is less than 100 sec. In the de Szoeke and Rhines model

$$c_0 u_*^2 \frac{dh}{dt} \sim 2m_0 u_*^3 \quad \text{or} \quad \frac{dh}{dt} \propto u_* \qquad (4\text{-}5)$$

This (C)$\sim$(D) balance for both models implies that the initial deepening proceeds due to turbulent motion in the mixed layer.

After this period, approximately from t=5 mins to t=18 mins, there is no simple balance in the Garwood solution. Therefore, the full form of the turbulent kinetic energy equation is required during this period. However, in the de Szoeke and Rhines model, a balance between (A) and (D) holds rather clearly from the early stage to about 1.2 hrs. For the Garwood model, this is the period that the value of nonstationarity is decreasing and entrainment shear production is increasing, although both the entrainment damping and the production minus dissipation are increasing to offset the value of non-stationarity and shear production. From t=18 mins to about t=12hrs, a balance (A)$\sim$(B) holds for the Garwood model,

$$\frac{1}{2}N^2h^2\frac{dh}{dt} \sim |\Delta C|^2\frac{dh}{dt}$$

or

$$R_i = \frac{|\Delta C|^2}{h\Delta b} \sim 1 \qquad (4\text{-}6)$$

This is the regime in which the bulk gradient Richardson numbers is nearly constant ($R_i \simeq 1$). For this time domain, the value of nonstationarity is decreasing and the strong shear production is balanced by the entrainment damping. In the de Szoeke and Rhines model, this balance (A)$\sim$(B)

holds from t=1.2 hrs to 8.8 hrs, which is somewhat shorter period compared to the Garwood model. Finally following t=12 hrs, a balance (A)~(D) holds for the Garwood model

$$\frac{1}{2}N^2h^2\frac{dh}{dt} \sim 2m u_*^3 - 2(\langle \bar{E} \rangle^{3/2} + f h \langle \bar{E} \rangle) \qquad (4\text{-}7)$$

Likewise in the de Szoeke and Rhines model, the same balance (A)~(D) holds although this begins earlier at t=8.8 hrs.

V. SUMMARY

The one-dimensional model of the ocean mixed layer of Garwood (1976, 1977) has been further generalized. The entrainment buoyancy flux equation in this model is derived from the turbulent kinetic energy budget at the base of the mixed layer. In earlier models, the unsteady term has been considered to be negligible in the derivation of the entrainment buoyancy flux equation. From the reduced form of the turbulent kinetic energy equation in which a balance holds among the shear production, the dissipation and the unsteady terms, Garwood (1976) nondimensionalized and solved this equation linearly using a constant dissipation time scale. He suggested that if the quasi-steady state assumption is made to facilitate solution, without filtering the surface boundary conditions, an incorrect high frequency response will not only be present but will bias the mean trend. Following these suggestions, the unsteady term has been included in the parameterization of entrainment buoyancy flux equation. Even though the entrainment buoyancy flux equation of the Garwood model is sufficient in most cases, this new generalized equation is necessary to study the asymptotic regimes.

To examine the importance of the unsteady term in the kinetic energy equation in more detail, the same reduced form as the Garwood (1976) equation is nondimensionalized, and

solved numerically using a nonconstant dissipation time scale, $\tau_\epsilon = h/\langle \bar{\epsilon} \rangle^{1/2}$. Solutions for variable amplitudes of fluctuation and forcing frequencies were obtained and their results are as follows. After an initial adjustment period $0 < \frac{u_* t}{h} < 4$:

i) For any amplitude of fluctuations, the quasi-steady state assumption may be good, if $\omega h/u_* < 0.02\pi$.

ii) In the case where the amplitude of the fluctuation is smaller than a half of the mean amplitude or $\omega h/u_* < .2\pi$ (i.e., $\tau_F >$ 10) the assumption of quasi-steady state may be possible.

iii) For the frequency $\omega h/u_* > .2\pi$, or the amplitude being larger than one-half of the mean amplitude, the unsteady term should not be neglected.

Following the lead of de Szoeke and Rhines (1976) and Niiler (1975), the relative contributions of entrainment damping, entrainment shear production, nonstationarity, wind shear production and dissipation were examined. The specific differences between two models are:

i) The Garwood model is computed implicitly for each term whereas the de Szoeke and Rhines' model is solved explicitly.

ii) Even with assumption of $\langle \bar{E} \rangle / u_*^2$ = a constant, an additional term $h \frac{d\langle \bar{E} \rangle}{dt}$ is in the Garwood model for the non-stationarity term (C).

iii) Dissipation is parameterized in a different manner, that is, Niiler (1975) parameterized the dissipation term as a fraction of near-surface production term, whereas Garwood (1976, 1977) parameterized the dissipation term in relating to net production. The numerical solutions of both models indicate that larger entrainment damping occurs in the de Szoeke and Rhines case inspite of smaller shear production compared to Garwood. Also, the solutions indicate that a larger nonstationarity term occurs in the Garwood model, and that a constant production minus dissipation term occurs in the de Szoeke and Rhines model compared to large variation in the Garwood model including the negative value of this term.

Following the method of de Szoeke and Rhines, each asymptotic regime is classified for both of the models.

i) From the initial instant to about 5 mins. a balance between the nonstationarity and the production minus dissipation holds in the Garwood model, i.e.,

$$\underset{(C)}{\frac{d(h\bar{E})}{dt}} \sim \underset{(D)}{2m u_*^3 - 2(\langle \bar{E} \rangle^{3/2} + fh\langle \bar{E} \rangle)}$$

This same balance holds in de Szoeke and Rhines with duration from the initial instant to about less than 100 sec.

ii) From t=5 mins to t=18 mins, a balance holds for the full form of the turbulent kinetic energy equation, whereas in the de Szoeke and Rhines model, a balance between the

entrainment damping and the entrainment shear production holds;

$$\underset{(A)}{\tfrac{1}{2}N^2h^2\frac{dh}{dt}} \sim \underset{(B)}{|\Delta \vec{v}|^2\frac{dh}{dt}}$$

or

$$Ri = \frac{|\Delta \vec{v}|^2}{h\Delta b} \sim 1$$

This balance (A)$\sim$(B) holds also in the de Szoeke and Rhines model from t=1.2 hrs to t=8.8 hrs.

iv) Following t=12 hrs, a balance between the entrainment damping and the production minus dissipation holds;

$$\underset{(A)}{\tfrac{1}{2}N^2h^2\frac{dh}{dt}} \sim \underset{(B)}{2m u_*^3 - 2(\langle \vec{E} \rangle^{3/2} + f h \langle \vec{E} \rangle)}$$

whereas in the de Szoeke and Rhines model, the same balance (A)$\sim$(D) holds, although this balance occurs a little earlier, from t=8.8 hrs.

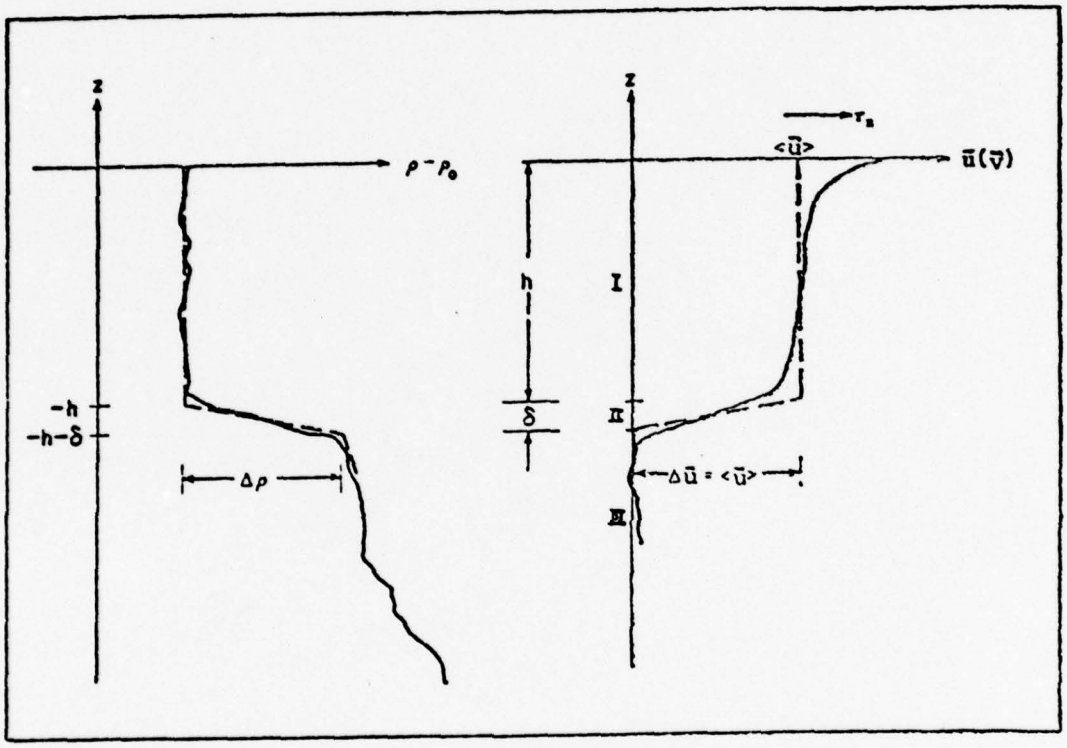

Figure 1. Idealized model for ocean mixed layer (----). Mixed layer depth is (h); (δ) is the thickness of the interface or entrainment zone. (Garwood(]976))

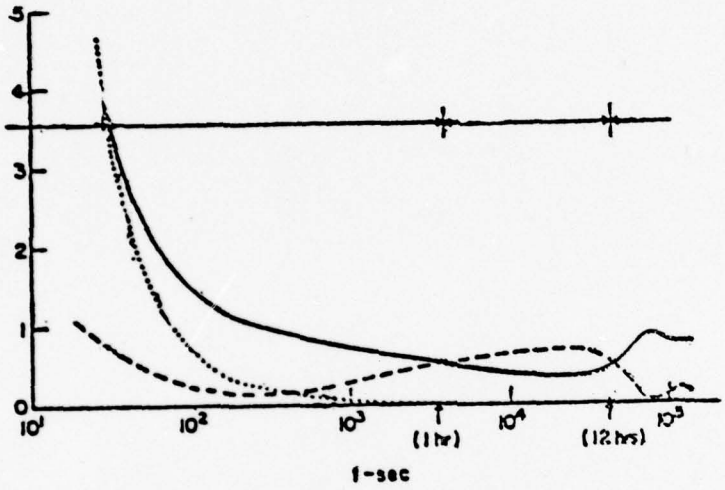

Figure 2. Numerical solution of the complete mixed layer model equation of de Szoeke and Rhines showing various asymptotic regimes. Solid curve: the ratio D/A of terms in the equation; dashed curve: B/A; dotted curve; C/A. Parameters $u_*=1, m_*=1, c_*=1$ (de Szoeke and Rhines(]976))

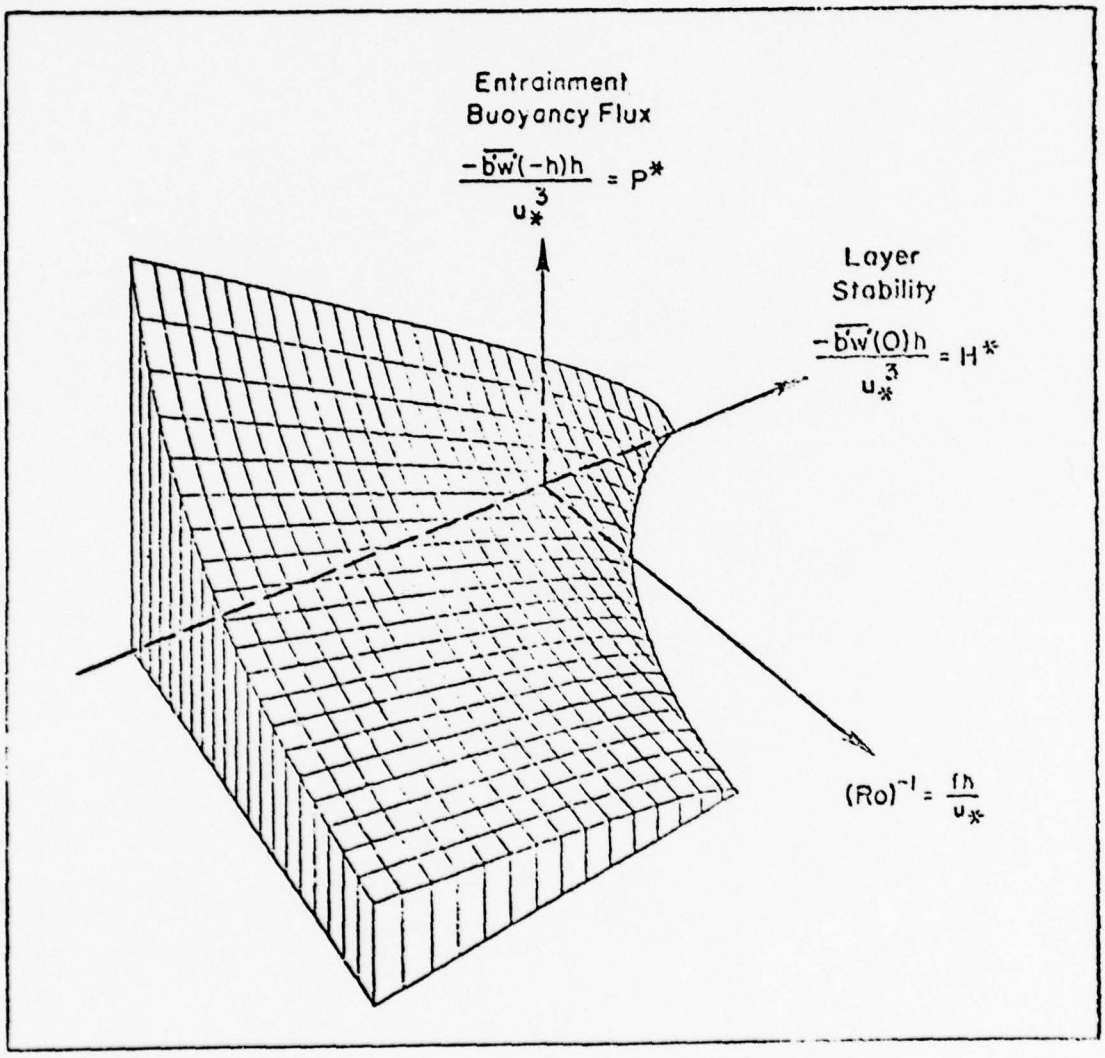

Figure 3. General solution to entrainment and turbulent kinetic energy equations. (Garwood(]976))

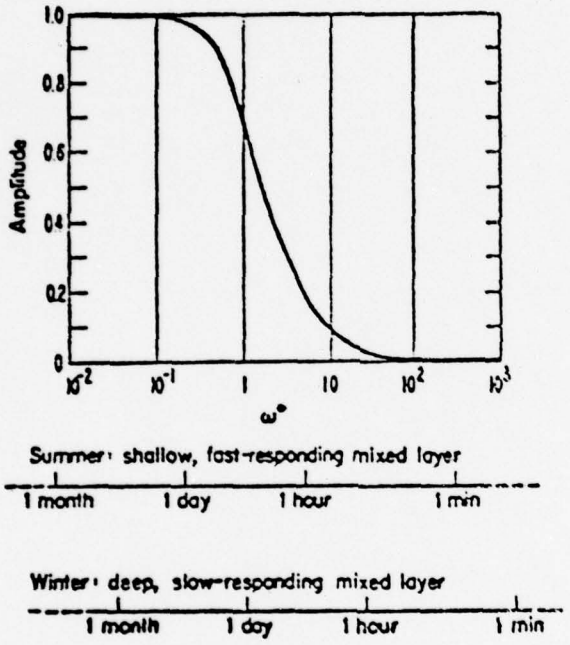

Figure 4. Response of the mixed layer to fluctuations in the surface boundary conditions; filtering effect. (Garwood(]976))

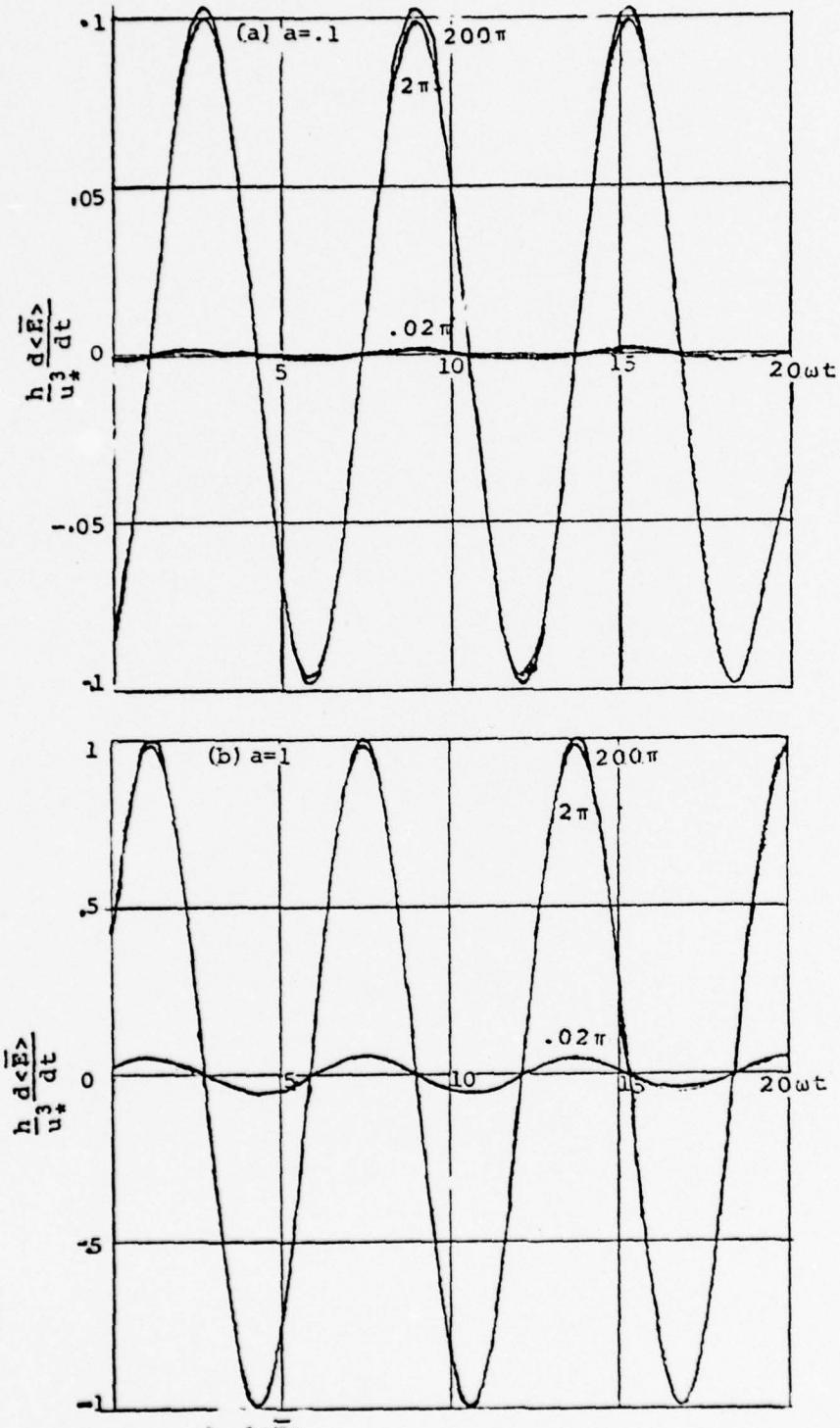

Figure 5. $\frac{h}{u_*^3}\frac{d<\bar{E}>}{dt}$ vs. ωt for three frequencies $\omega h/u_* = 200\pi, 2\pi$ and $.02\pi$.

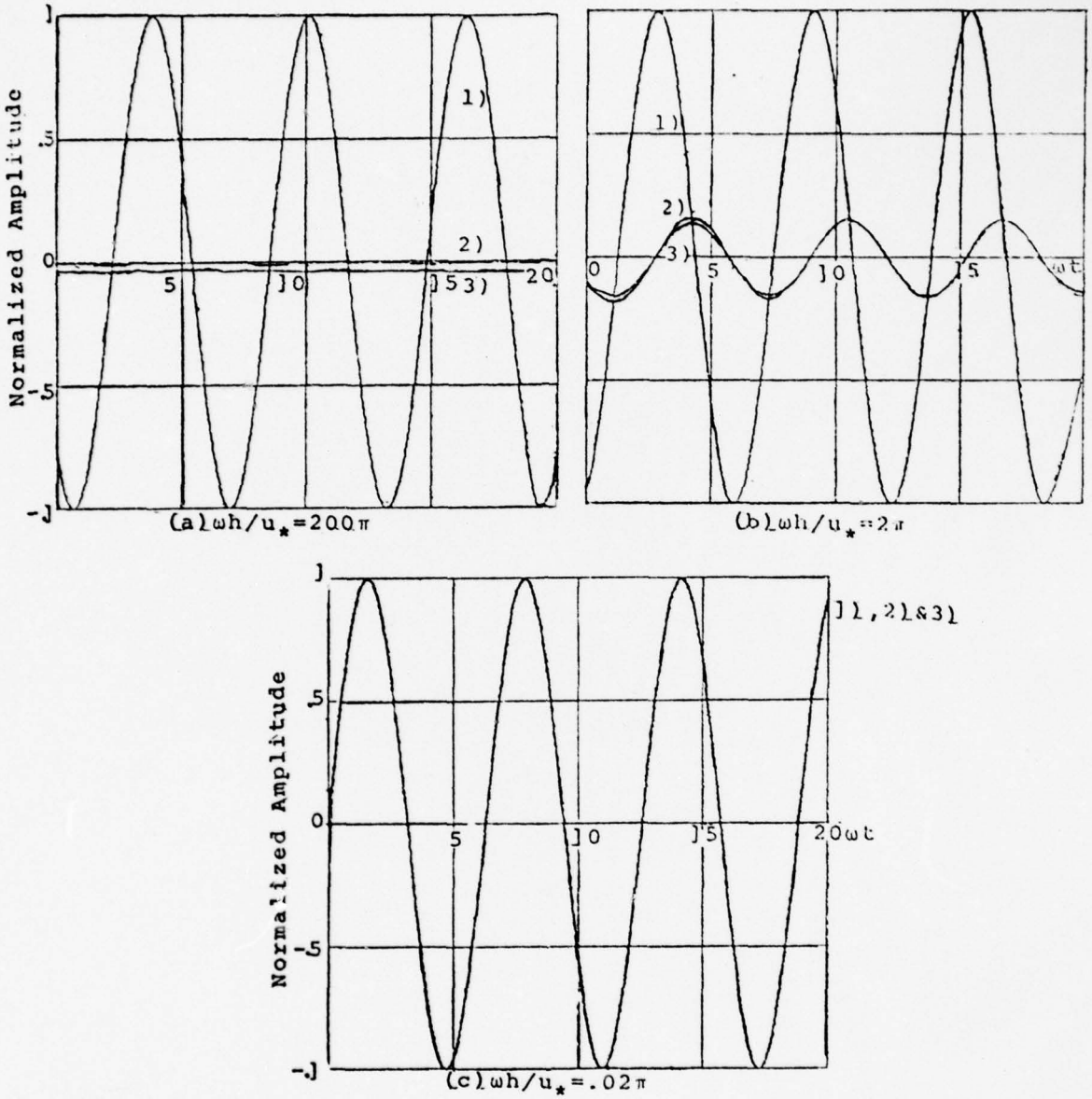

Figure 6. Comparison of following three cases for each non-dimensionalized frequency (a) $\omega h/u_* = 200\pi$, (b) 2π and (c) $.02\pi$.

Case 1) $\sin\omega t$ function of the wind forcing vs. ωt.

Case 2) Fluctuating component of dissipation normalized in amplitude of wind production vs. ωt for for a=1.

Case 3) Same as case 2) except for a=.1.

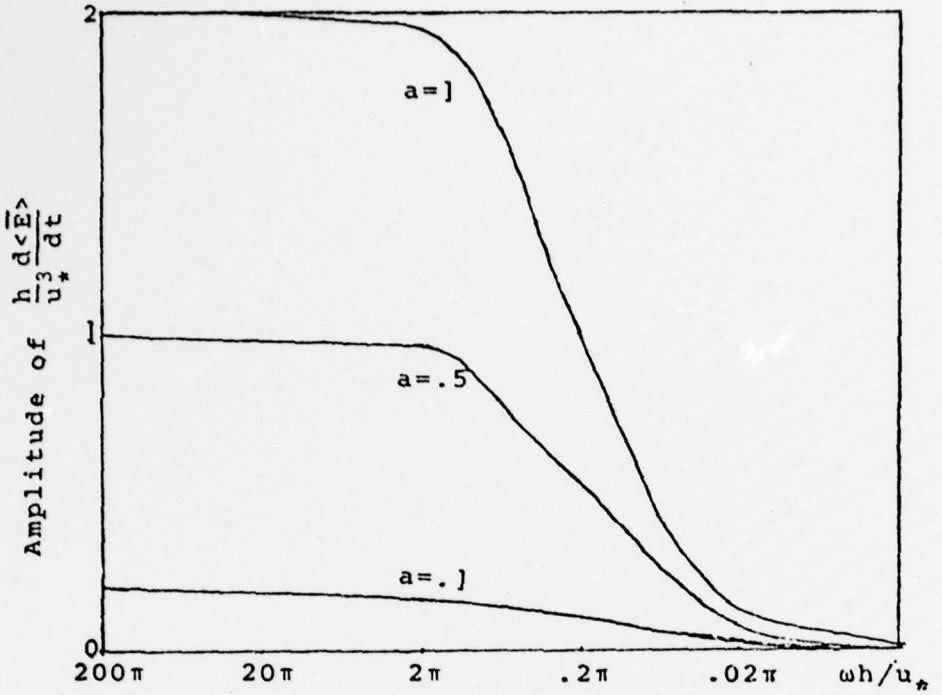

Figure 7. Peak to peak amplitude of unsteady term vs. nondimensionalized frequency.

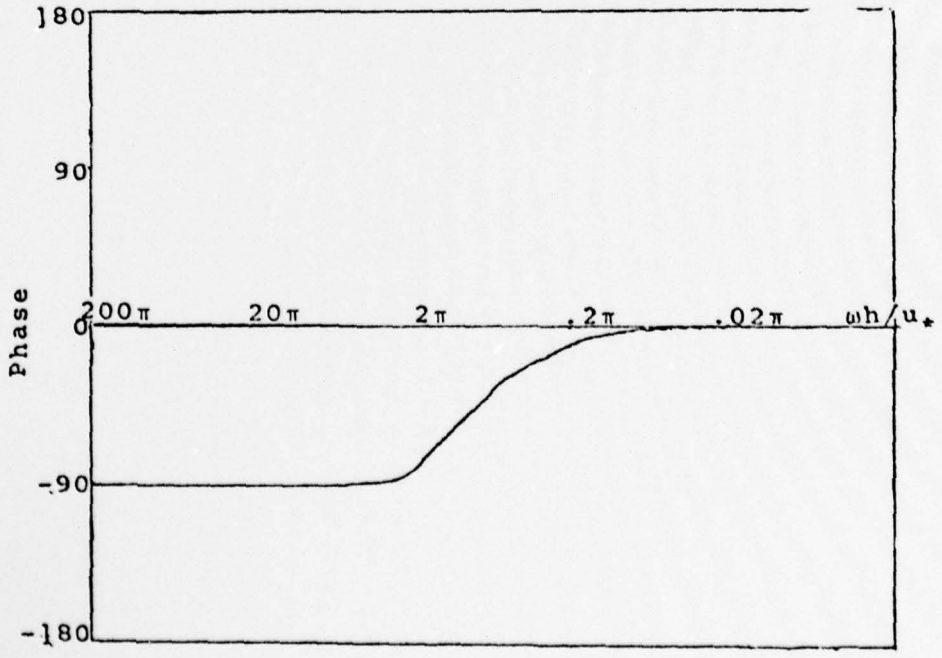

Figure 8. Phase difference between wind production and dissipation vs. nondimensionalized frequency

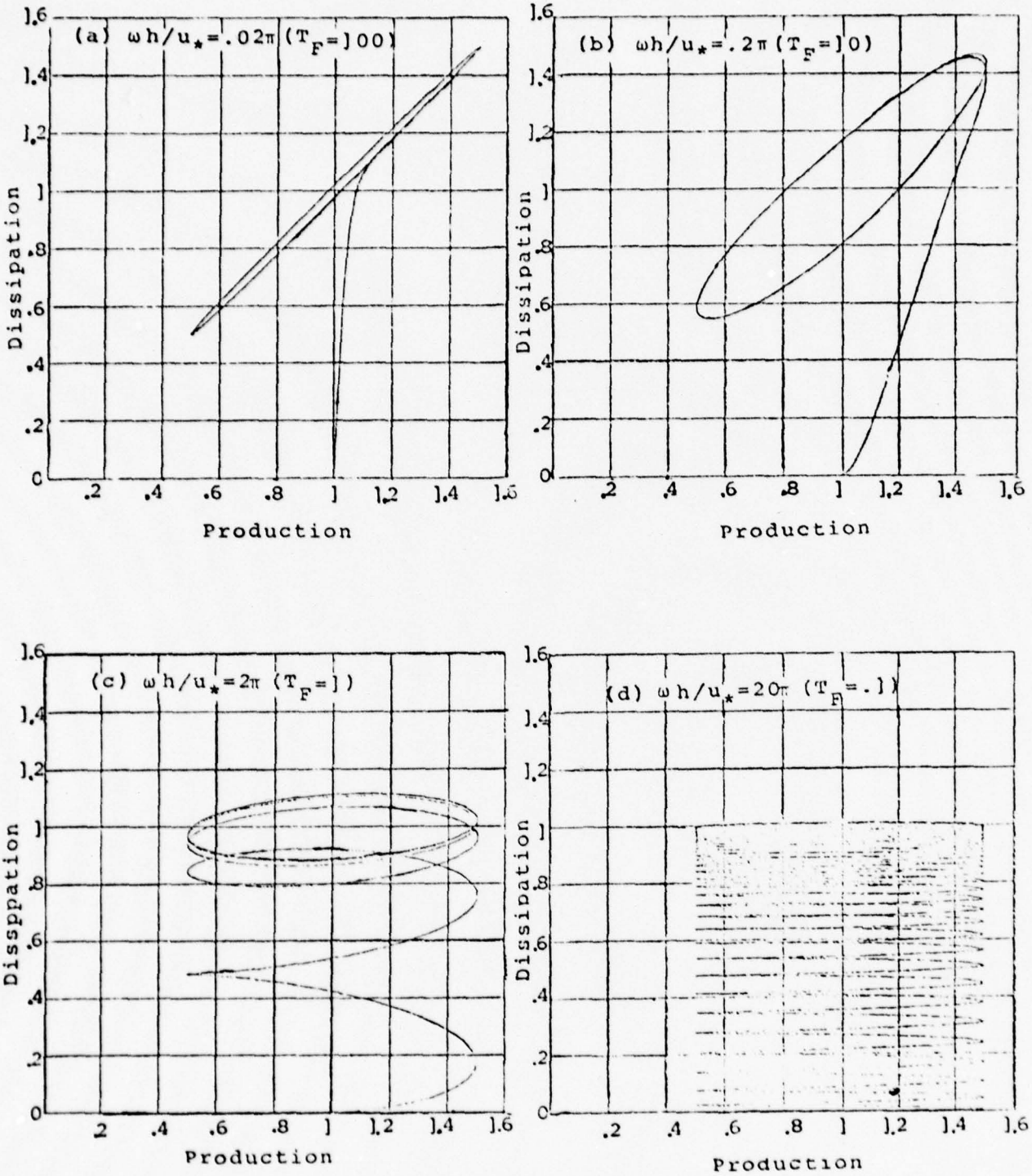

Figure 9. Nondimensional dissipation versus prescribed wind shear production for four periods of osciallation.

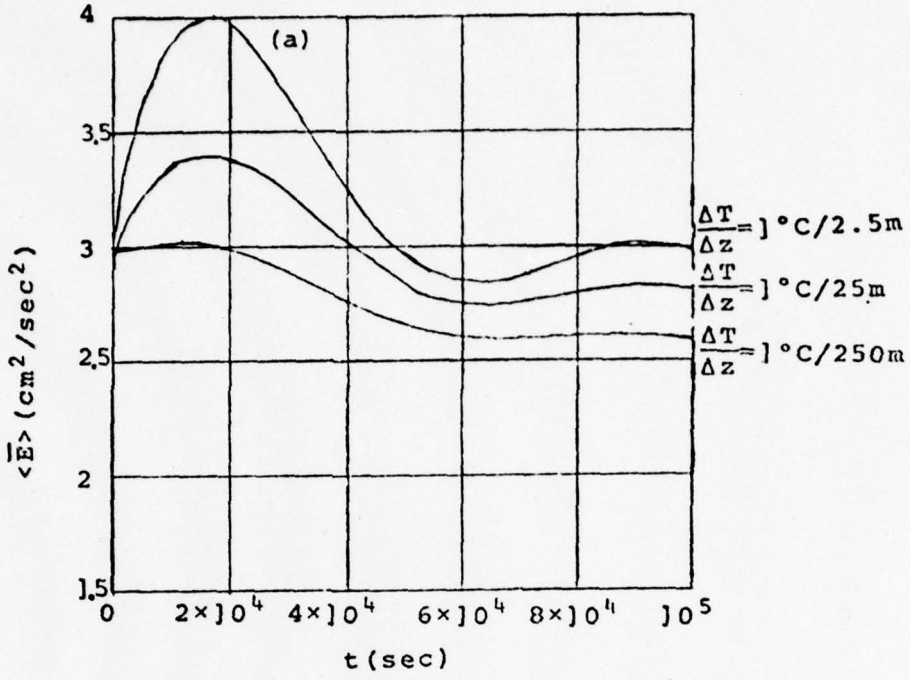

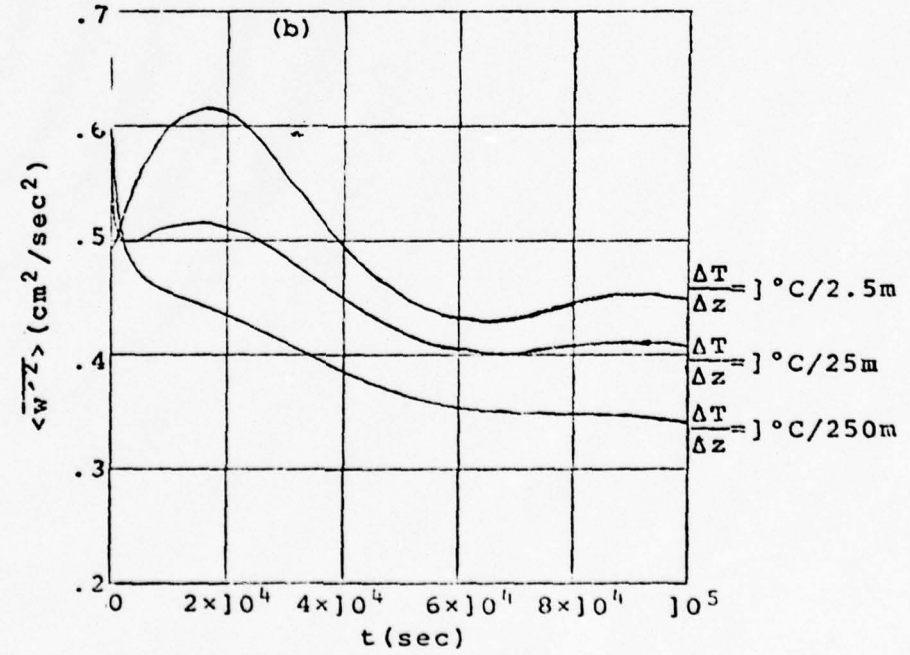

Figure 10. (a) Total turbulent kinetic energy and (b) Vertical component of turbulent kinetic energy versus time for lapse rate 1°C/2.5m, 1°C/25m and 1°C/250m.

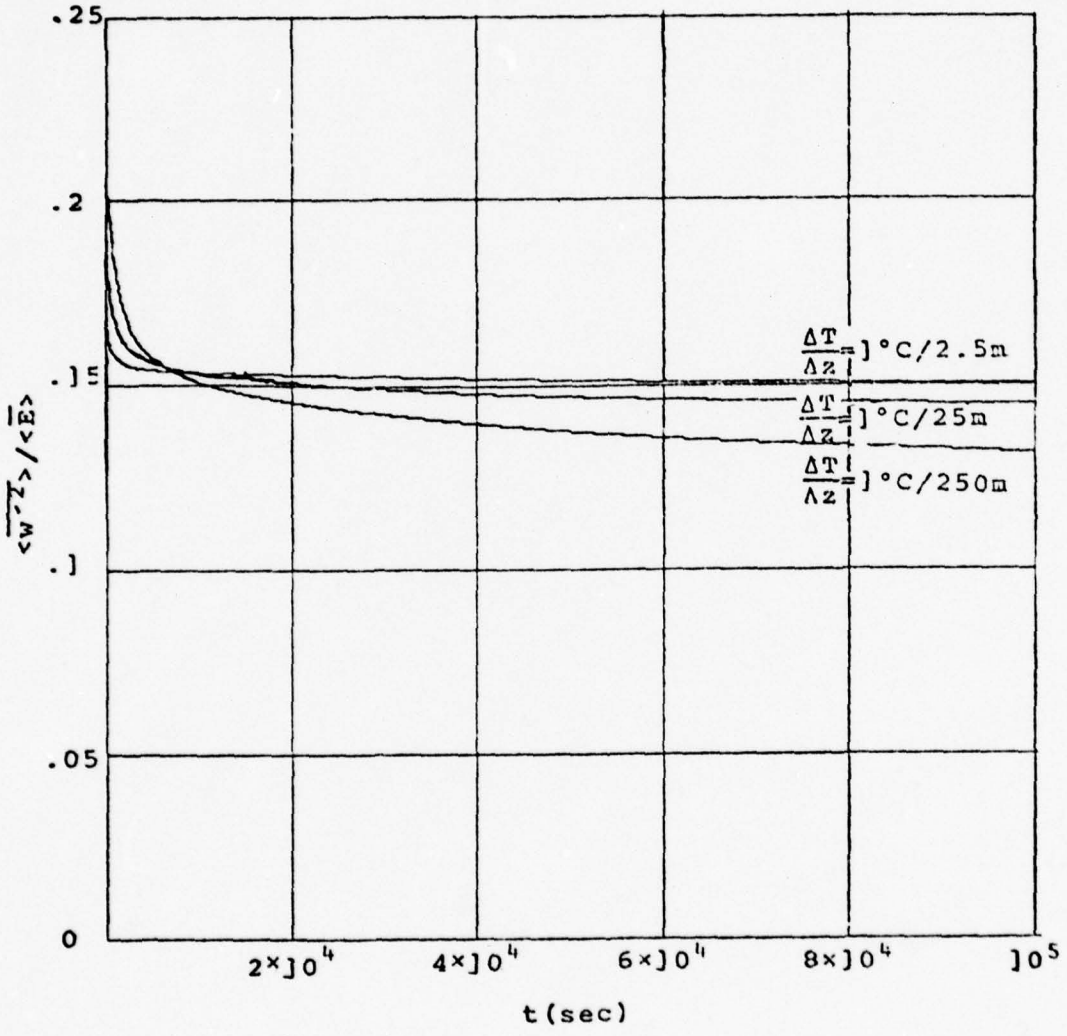

Figure 11. $\overline{\langle w'^2 \rangle}/\langle \bar{E} \rangle$ versus time

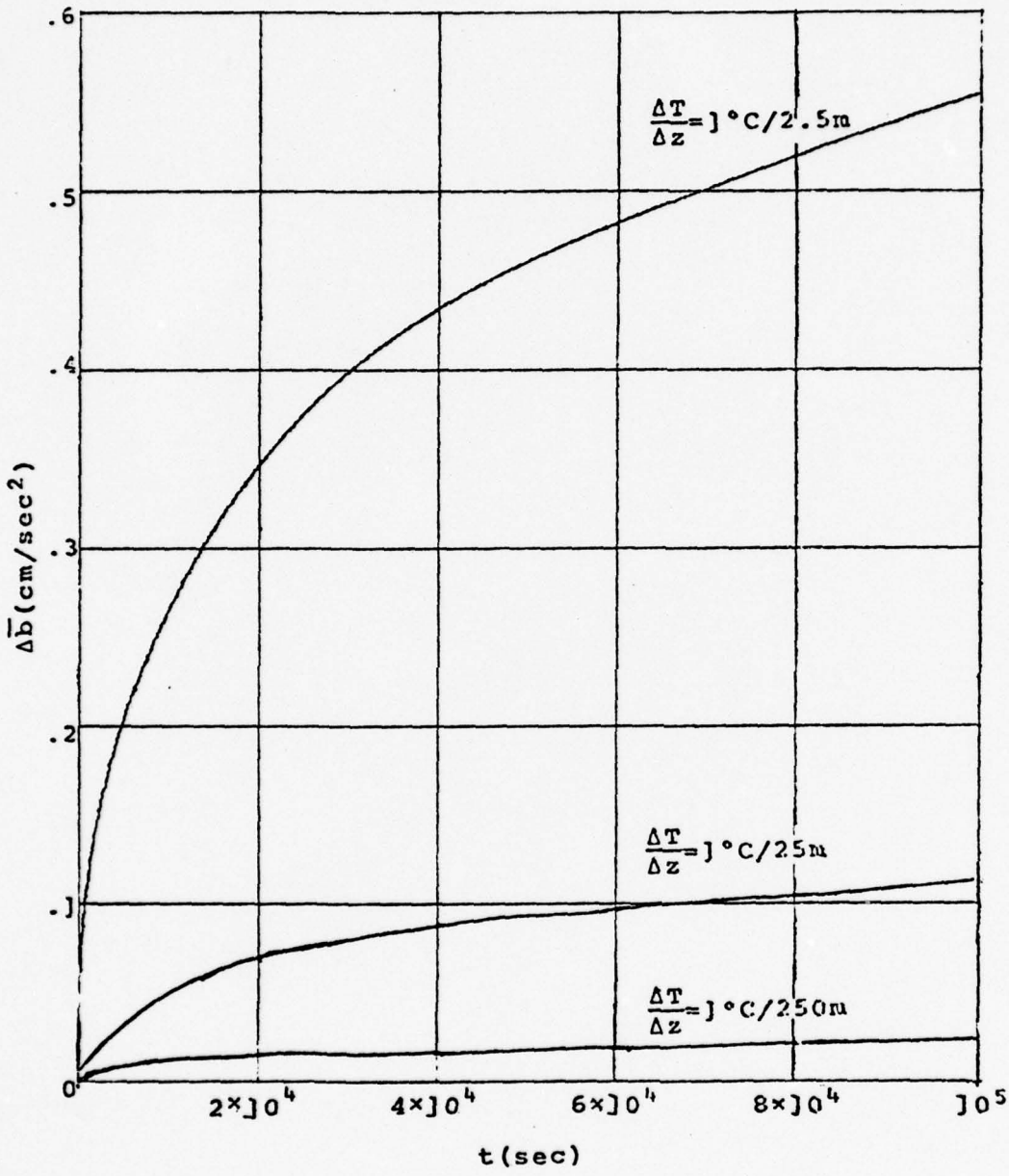

Figure 12. $\Delta\bar{b}$ vs. time for lapse rate 1°C/2.5m, 1°C/25m and 1°C/250m.

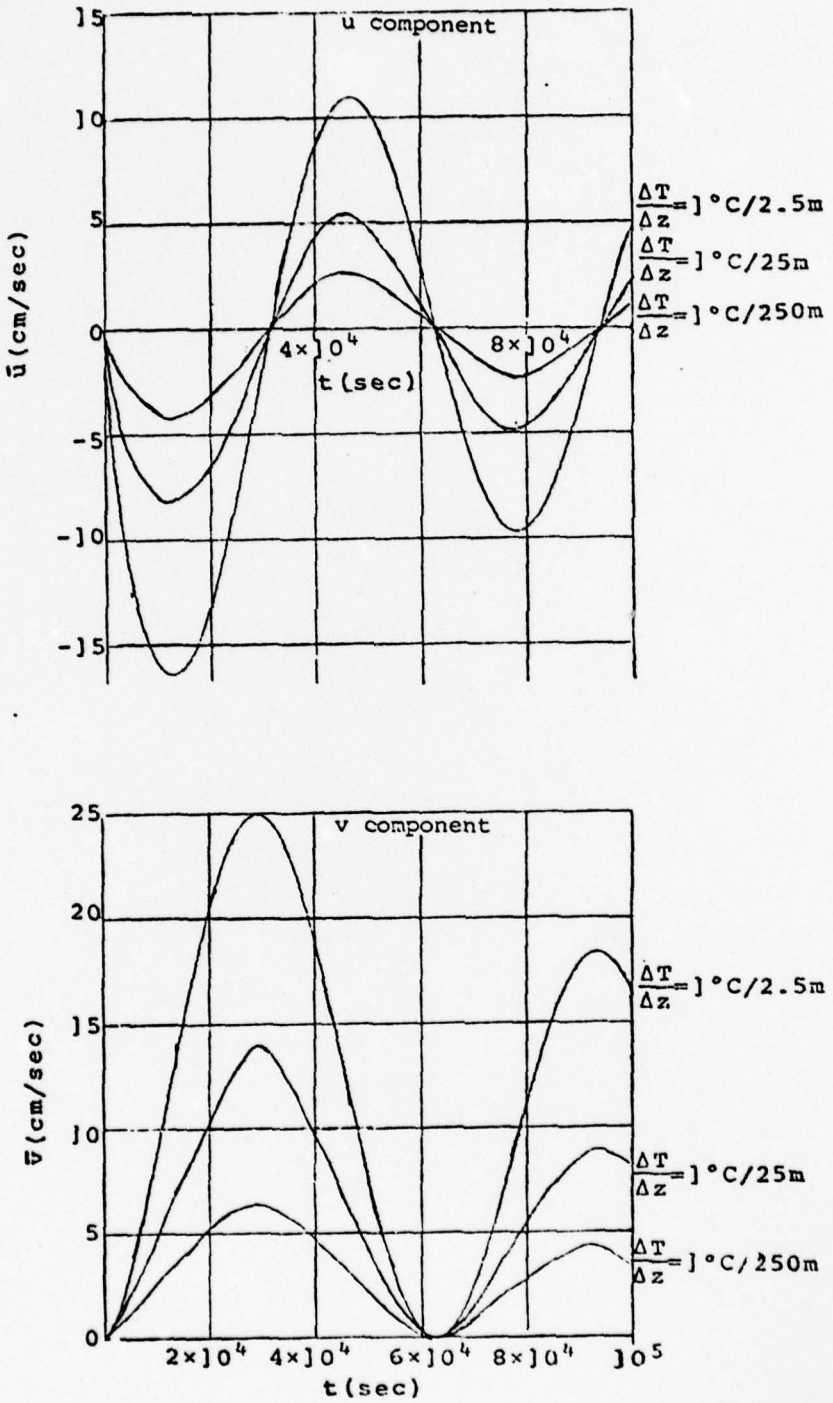

Figure 13. u and v component of mean velocity for lapse rate 1°C/2.5m, 1°C/25m and 1°C/250m.

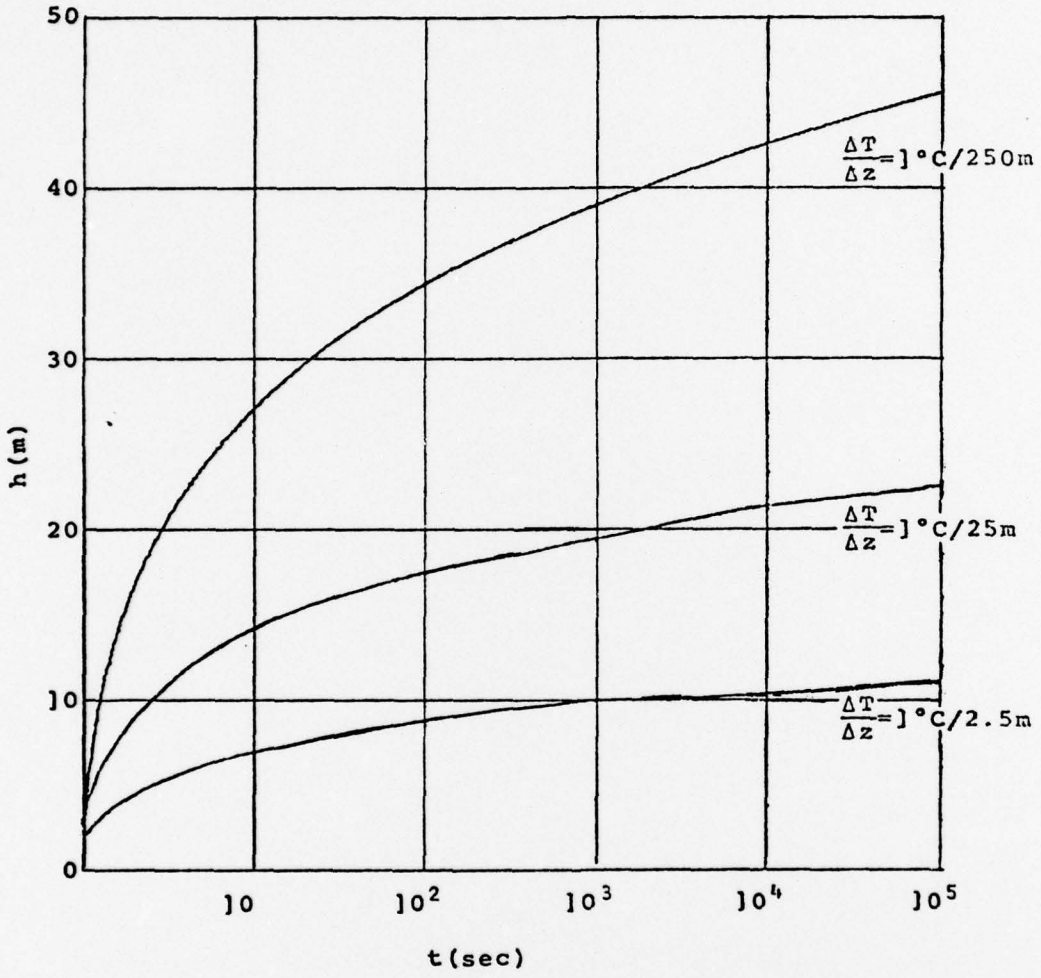

Figure 14. Mixed layer depth vs. time for lapse rate 1°C/2.5m, 1°C/25m and 1°C/250m.

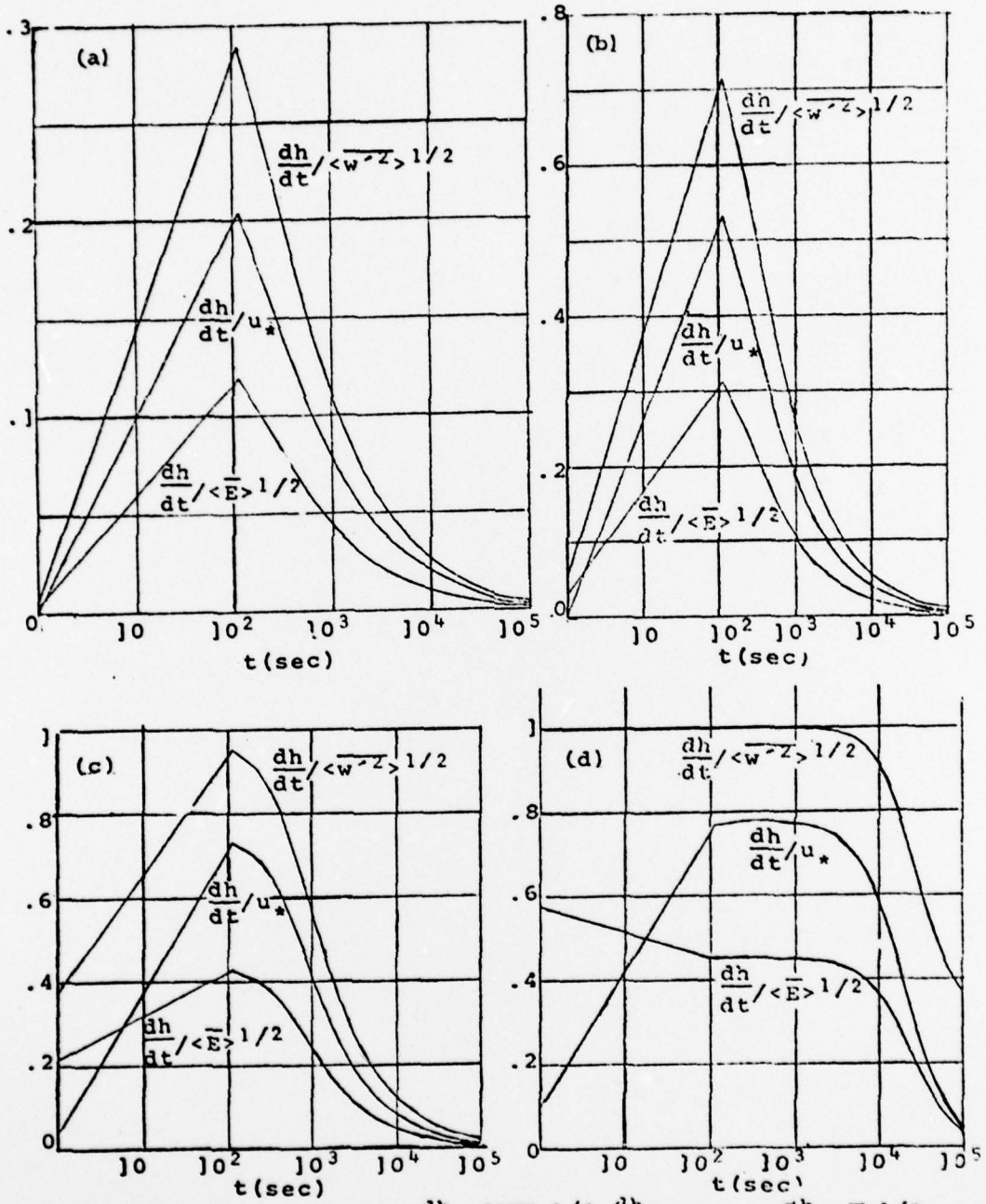

Figure 15. Comparison of $\frac{dh}{dt}/\langle\overline{w'^2}\rangle^{1/2}$, $\frac{dh}{dt}/u_*$ and $\frac{dh}{dt}/\langle\bar{E}\rangle^{1/2}$ for lapse rate (a)1°C/2.5m, (b)1°C/25m, (c)1°C/250m and (d)1°C/250000m.

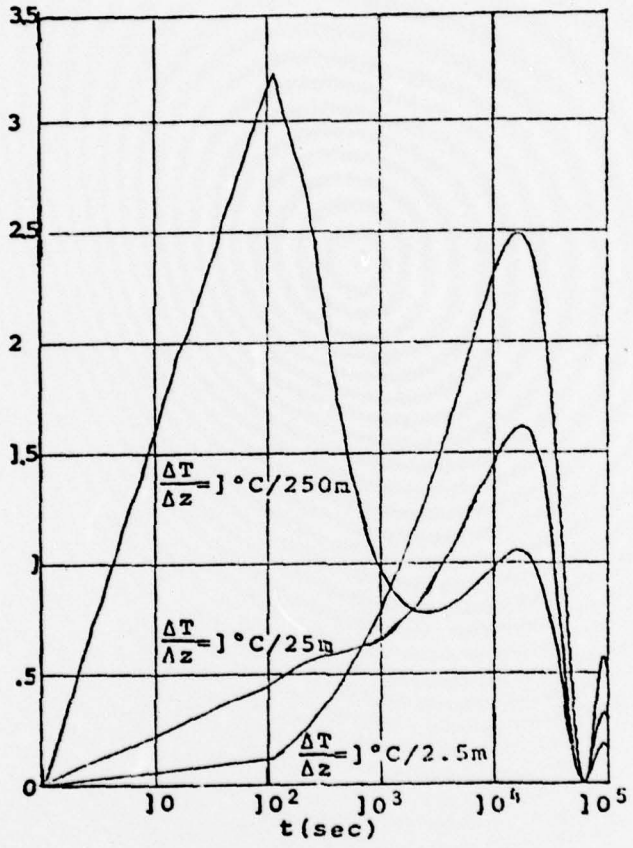

Figure 16. $Ri^{-1}=\frac{\overline{u}^2+\overline{v}^2}{h\Delta b}$ vs. time for lapse rate 1°C/2.5m, 1°C/25m and 1°C/250m.

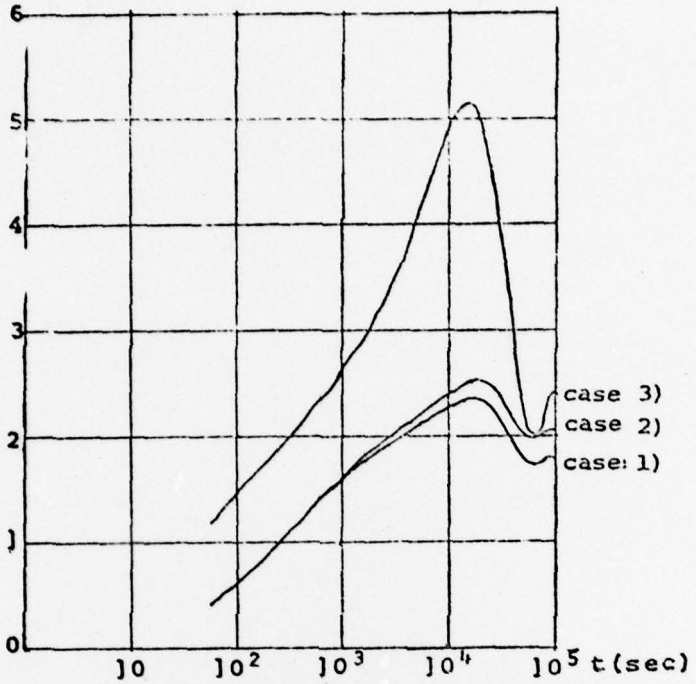

Figure 17. Comparison of the entrainment damping term in three cases

Case 1) Garwood--full equations.

Case 2) Garwood--without planetary scale dissipation.

Case 3) de Szoeke and Rhines.

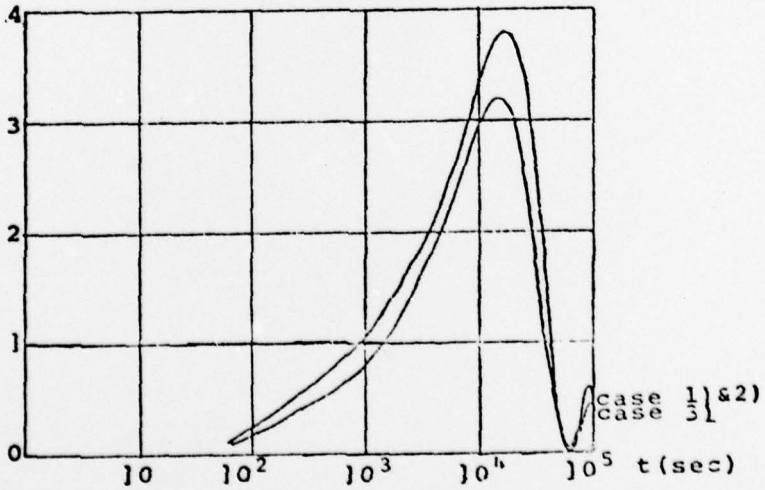

Figure 18. Comparison of the entrainment shear production term in the same three cases as in figure 17.

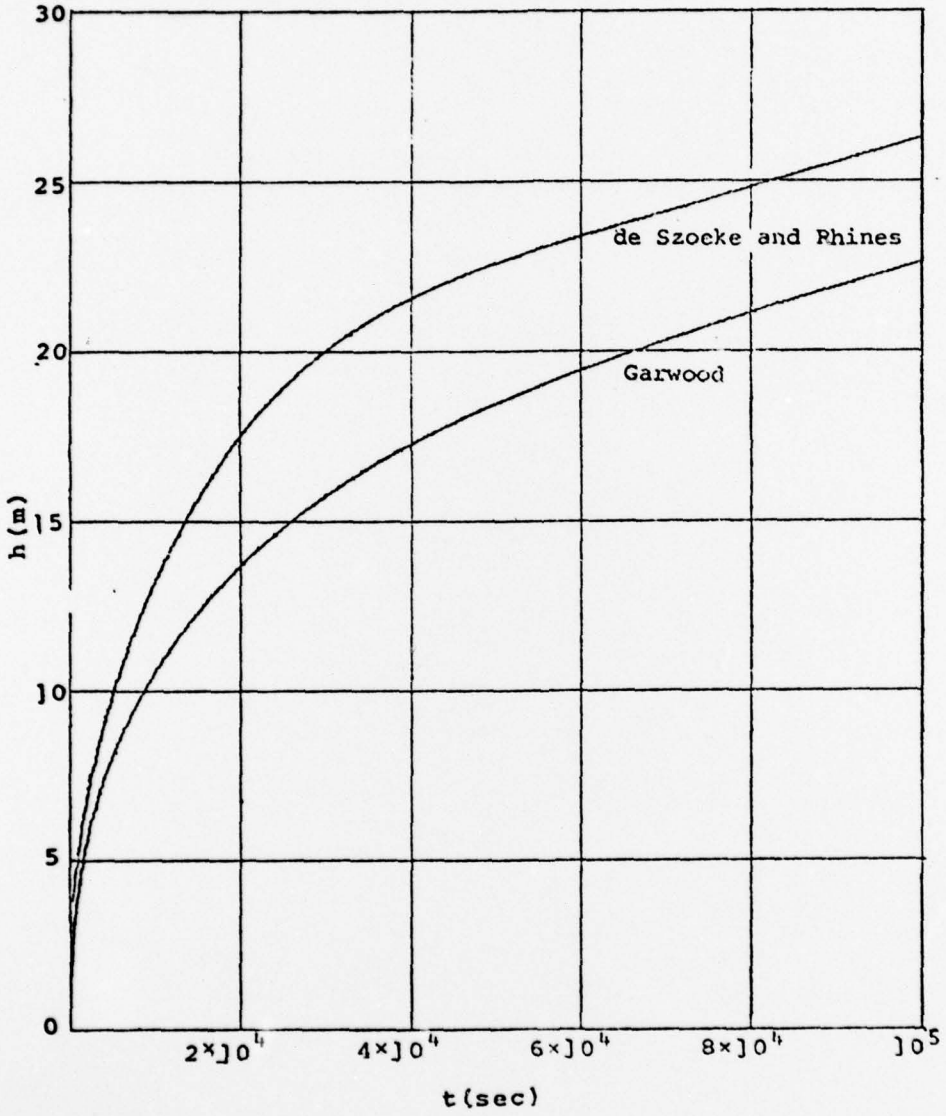

Figure 19. Mixed layer depth versus time.

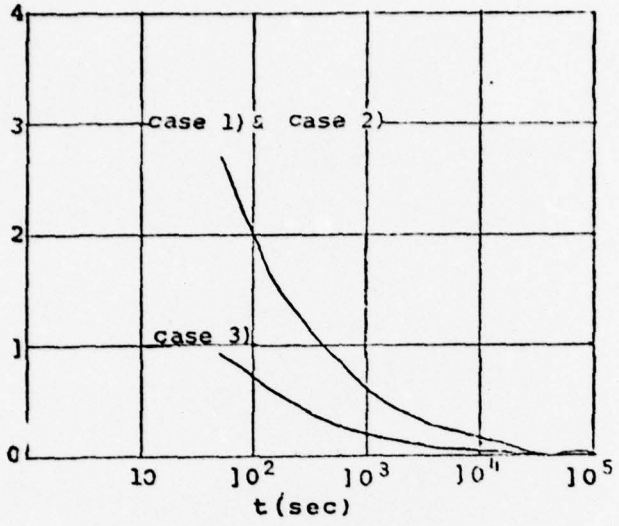

Figure 20. Comparison of the nonstationarity term in the same three cases as in figure 17.

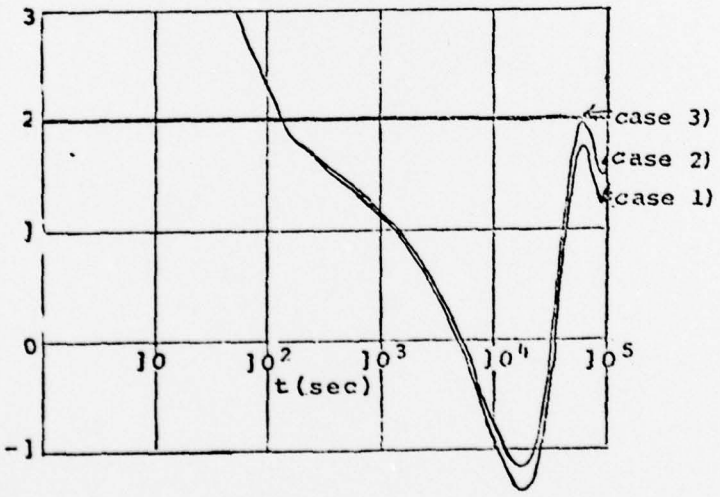

Figure 21. Comparison of the production minus dissipation term in the same three cases as in figure 17

Figure 5. $\frac{h}{u_*^3}\frac{d\langle E\rangle}{dt}$ vs. ωt for three frequencies $\omega h/u_* = 200\pi, 2\pi$ and $.02\pi$.

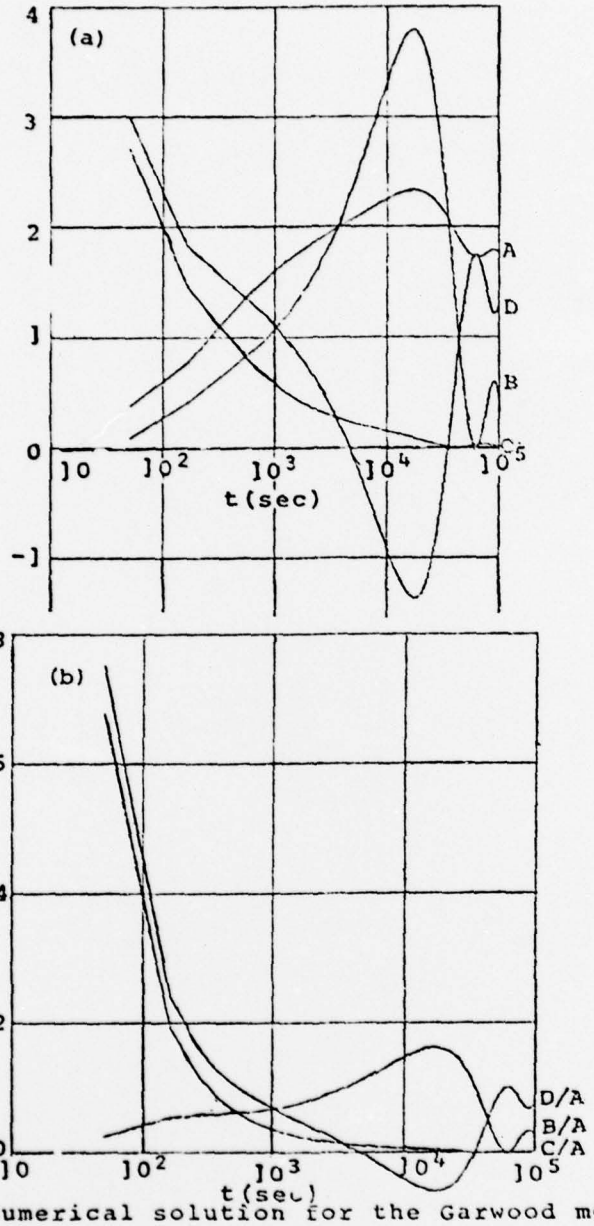

Figure 22. Numerical solution for the Garwood model (b) in terms of B/A, C/A and D/A. Parameters and boundary conditions: $m=6$, $f=10^{-4}\,sec^{-1}$, $\Gamma=N^2=10^{-4}\,sec^{-2}$, $\overline{u'v'}=1\,cm^2/sec^2$, $\overline{v'w'}=0$, $\overline{b'w'}=0$, $u_*=1$ cm/sec, Initial conditions: $h=100$cm, $\langle\bar{E}\rangle=.03$ cm^2/sec^2, $\langle\overline{w'^2}\rangle=.01\,cm^2/sec^2$, $\Delta\bar{b}=5\times10^{-3}\,cm/sec^2$.

Case 3) Same as case 2) except for a=.].

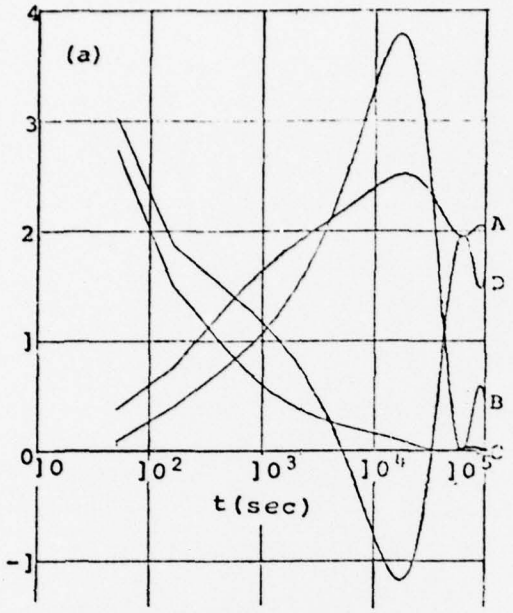

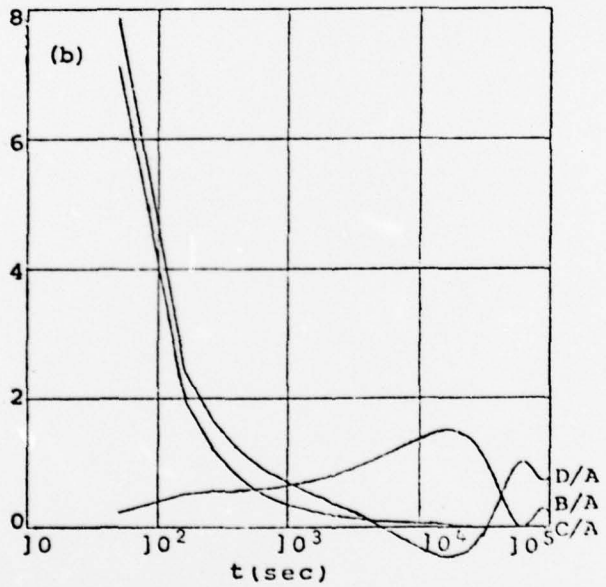

Figure 23. Numerical solution for the Garwood model without the planetary scale dissipation term (a) in terms of A,B,C and D separately, and (b) in terms of B/A,C/A and D/A. Parameters and conditions are the same as in figure 22.

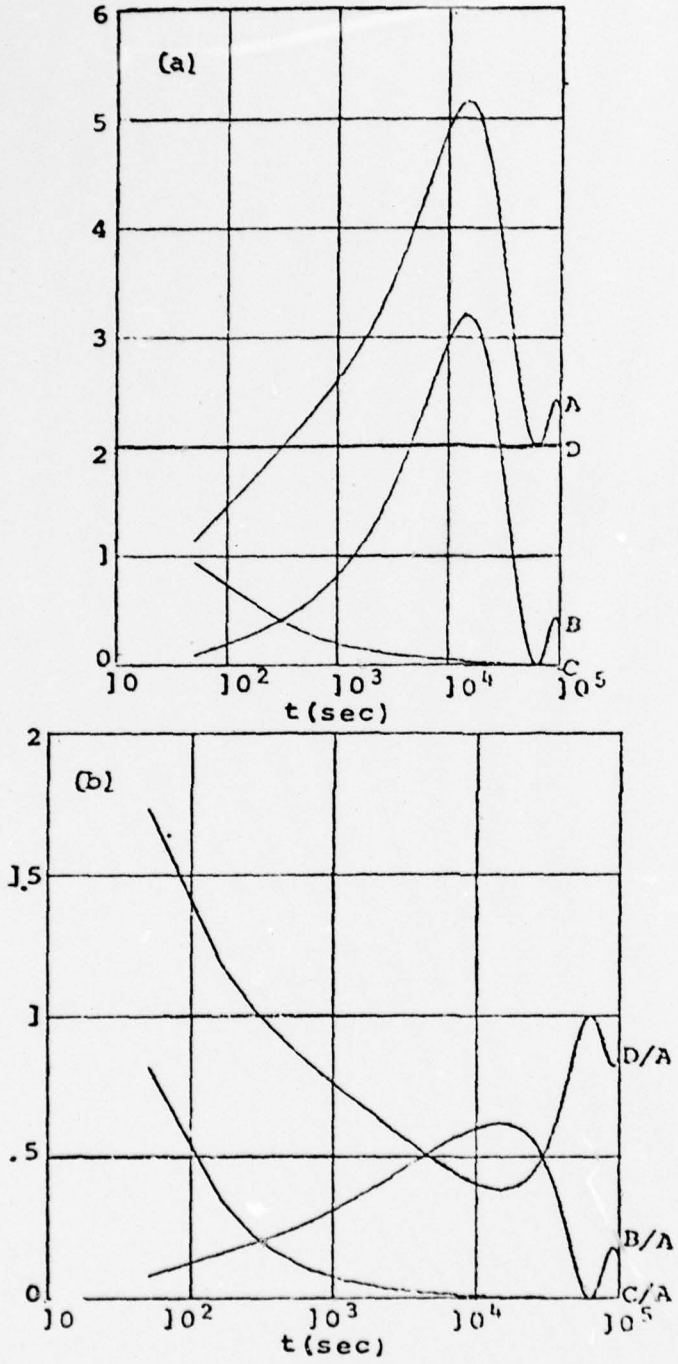

Figure 24 Numerical solution for the de Szoeke and Rhines' model (a) in terms of A,B,C and D separately, and (b) in terms of B/A,C/A and D/A. Parameters: $m_o=c_o=1$, $u_*=1$cm/sec, $f=10^{-4}$ sec^{-1}, $\Gamma=N^2=10^{-4}sec^{-2}$, Initial condition: h=100cm.

LIST OF REFERENCES

1. Denman, K. L., "A Time Dependent Model of the Upper Ocean," J. Phys. Oceanogr., v. 3, p. 173-184, 1973.

2. de Szoeke, R. A., and P. B. Rhines, "Asymptotic Regimes in Mixed Layer Deepening," J. Marine Res., v. 34, p. 111-116, 1976.

3. Ekman, V. W., "On the Influence of the Earth's Rotation on Ocean Currents," Ark. Mat. Astron. Fys., v. 2(11), p. 1-53, 1905.

4. Elsberry, R. L., T. S. Fraim and R. N. Trapnell, "A Mixed Layer Model of the Oceanic Thermal Response to Hurricanes," J. Geophys. Res., v. 81, p. 1153-1162, 1976.

5. Garwood, R. W., A General Model of the Ocean Mixed Layer Using a Two-component Field Closure, Ph. D. Thesis, University of Washington, NOAA Tech. Report ERL 384-PMEL 27), 1976.

6. Garwood, R. W., "An Oceanic Mixed Layer Model cable of Simulating Cyclic States," J. Phys. Oceanogr., v. 7, p. 455-468, 1977.

7. Halpern, D., "Observations of the Deepening of the Wind Mixed Layer in the Northeast Pacific Ocean," J. Phys. Oceanogr., v. 4, p. 454-466, 1974.

8. Kato, H., and O. M. Phillips, "On the Penetration of a Turbulent Layer into Stratified Fluid," J. Fluid Mech., v. 37, p. 643-655, 1969.

9. Kim, J., "A Generalized Bulk Model of the Oceanic Mixed Layer," J. Phys. Oceanogr., v. 6, p. 686-695, 1976.

10. Kitaigoradsky, S. A., "On the computation of the thickness of the wind-mixing layer in the ocean," Bull. Acad. Sci. U. S. S. R. Geophys. Ser., v. 3, p. 284-287, 1960.

11. Kraus, E. B., Modeling and Prediction of the Upper Layers of the Ocean, The Pergamon Press, 1975.

12. Kraus, E. B., and J. S. Turner,"A One-dimensional Model of the Seasonal Thermocline" Part II, Tellus, v. 19, p. 98-105, 1967.

13. Miropol'skiy, Yn. A., "Nonstationary Model of the Wind-Convection Mixing Layer in the Ocean," Izv. Atmos. Oceanic Phys., v. 6, pg. 1284-1294, 1970.

14. Niiler, P. P., "Deepening of the Wind Mixed Layer," J. Mar. Res., v. 33, p. 405-422, 1975.

15. Pollard, R. T., P. B. Rhines and R. Thompson, "The Deepening of the Wind-Mixed Layer," Geophys. Fluid Dyn., v. 3, p. 381-404, 1973.

16. Rossby, C. G., and R. B. Montgomery, "The Layer of Frictional Influence in Wind and Ocean Currents," Pap. Phys. Oceanogr. Meter., v. 3, no. 3, 1935.

17. Tennekes, H., and J. L. Lumley, A First Course in Turbulence, MIT Press, 1972.

18. Zeman, O., and H. Tennekes, "Parameterization of the Turbulent Energy Budget at the Top of the Daytime Atmospheric Boundary Layer," J. Atmos. Sci., v. 34, p. 111-123, 1977.

19. Zilitinkevich, S. S., "Comments on 'A model for the dynamics of the inversion above a convective boundary," J. Atmos. Sci., v. 32, p. 991-992, 1975.

INITIAL DISTRIBUTION LIST

		No. Copies
1.	Defense Documentation Center Cameron Station Alexandria, Virginia 22314	2
2.	Library, Code 0142 Naval Postgraduate School Monterey, California 93940	2
3.	Director Naval Oceanography and Meteorology National Space Technology Laboratories Bay St. Louis, Mississippi 39520	1
4.	Professor R. W. Garwood, Code 68Gd Department of Oceanography Naval Postgraduate School Monterey, California 93940	8
5.	Chairman, Department of Oceanography, Code 68 Naval Postgraduate School Monterey, California 93940	3
6.	Professor G. J. Haltiner, Code 63Ha Chairman, Department of Meteorology Naval Postgraduate School Monterey, California 93940	1
7.	Lieutenant J. Y. Yun Korean Naval Academy Jin Hae, Kyung-Nam, Korea	2
8.	Professor R. L. Elsberry, Code 63Es Department of Meteorology Naval Postgraduate School Monterey, California 93940	1
9.	Professor R. L. Haney, Code 63Hy Department of Meteorology Naval Postgraduate School Monterey, California 93940	1
10.	ADCNO for Education & Training Div. Naval HQ Dae Bang-Dong, Kwanak-ku Seoul, Korea	1

11. Academic Dean — 1
Korean Naval Academy
Jin-Hae, Kyung-Nam, Korea

12. Dr. Jong-Wha Lee — 1
JinHae Research Laboratory
P. O. Box 18, JinHae, Kyung-Nam
Korea

13. Professor Yong-An Park — 1
Chairman, Department of Oceanography
Seoul National University
Kwanak-Ku, Seoul, Korea

14. Dr. Byung Don Lee — 1
Director, Korea Research Institute of Ocean
P. O. Box 151 Dong Dae Mun, 39-1, Hawolgok-Dong,
Sungbuk-ku, Seoul, Korea

15. Mr. Patrick C. Gallacher, Code 63Ga — 1
Department of Meteorology
Naval Postgraduate School

16. Oceanographer of the Navy, Code N-45 — 1
Hoffman Building No. 2
200 Stovall Street
Alexandria, Virginia 22332

17. Office of Naval Research — 1
Code 410
NORDA
NSTL Station, Mississippi 39529

18. Dr. Robert E. Stevenson — 1
Scientific Liaison Office, ONR
Scripps Institution of Oceanography
La Jolla, California 92037

19. Library, Code 3330 — 1
Naval Oceanographic Office
Washington, DC 20373

20. SIO Library — 1
University of California, San Diego
P. O. Box 2367
La Jolla, California 92037

21. Department of Oceanography Library — 1
University of Washington
Seattle, Washington 98105

22. Department of Oceanography Library 1
Oregon State University
Corvallis, Oregon 97331

23. Commanding Officer 1
Fleet Numerical Weather Central
Monterey, California 93940

24. Commanding Officer 1
Naval Environmental Prediction Research Facility
Monterey, California 93940

25. Department of the Navy 1
Commander Oceanographic System Pacific
Box 1390
Pearl Harbor, Hawaii 96860